THE UNIVERSITY OF MICHIGAN

COLLEGE OF ENGINEERING
Department of Mechanical Engineering
Heat Transfer and Thermodynamics Laboratory

Six Month Progress Report

AUTOMOTIVE RADIATORS MANUFACTURED BY THE ELECTROFORMING PROCESS

(Covering the Period Oct. 1, 1962 to Apr. 1, 1963)

John A. Clark
Clarence A. Siebert
Robert B. Keller
David M. Mellen
Jo C. Hoo

ORA Project 05335

under contract with:

INTERNATIONAL COPPER RESEARCH ASSOCIATION, INC.
NEW YORK, NEW YORK

administered through:

OFFICE OF RESEARCH ADMINISTRATION ANN ARBOR

May 1963

TABLE OF CONTENTS

NOMENCLATURE

English

A	total heat transfer area on one side, ft^2
A_c	minimum air side free flow area, ft^2
A_{FR}	total frontal area air side, ft^2
a	plate thickness, ft
b	plate spacing, ft
c_p	specific heat at constant pressure, Btu/lbm-°F
f	friction factor, dimensionless
G	mass velocity, (w/A_c), lbm/hr-ft^2
g_o	conversion factor; $g_o = 32.2$ (lbm/lbf)(ft/sec^2)
h	heat transfer coefficient, Btu/hr-ft^2-°F
k	thermal conductivity, Btu/hr-ft-°F
L	total flow length of heat exchanger, ft
NTU	number of transfer units, dimensionless
Pr	Prandtl number, dimensionless
q	heat transfer rate, Btu/hr
Re	Reynolds number, dimensionless
r_h	hydraulic radius $(A_c L/A)$, ft, $4r_h$ = hydraulic diam
St	Stanton number, dimensionless
T	temperature, °F
U	overall heat transfer coefficient, Btu/hr-ft^2-°F

V	volume, ft^3
V_B	air volume between plates, ft^3
w	mass flow rate, lbm/hr

Greek

α	ratio of total heat transfer area on one side to total volume of heat exchanger A/V, ft^2/ft^3
β	ratio of total heat transfer area on one side of a plate-fin heat exchanger to the volume of air between plates on that side, A/V_B, ft^2/ft^3
δ	water channel thickness, ft
ϵ	heat transfer effectiveness (Ref. 24), dimensionless
η_o	total surface temperature effectiveness, dimensionless
σ	A_c/A_{FR}, dimensionless
ρ	density, lbm/ft^3
μ	viscosity, lbm/ft-hr
ψ	see Eq. (22)

Subscripts

c	cold (air) side of heat exchanger
h	hot (water) side of heat exchanger
w	wall
max	maximum
min	minimum
i	inlet
o	reference heat exchanger.

ABSTRACT

This is a progress report covering the first six-month period of effort, Oct. 1, 1962, to Apr. 1, 1963, on research directed at the problems of manufacturing an air-water heat exchanger suitable for automotive application by the electroforming process. Such an exchanger would be constructed without soldered joints. The work has been divided into three parallel phases: (1) selection and evaluation of core designs; (2) a metallurgical study of the physical properties of electroformed copper sheets and electroformed copper joints; and (3) the production of an electroformed heat exchanger. Phase (1) and (2) are underway at The University of Michigan, and Phase (3) is being done at the Graham-Savage Associates, Electroformers of Kalamazoo, Michigan.

Eighteen different heat exchanger core configurations have been evaluated on the basis of their thermal performance and the most compact type identified. This design consists of the plate-fin core with the fins ruffled in order to promote the turbulent flow of air, thus providing improved heat transfer capability. Wind tunnel apparatus suitable for determining the experimental performance of an electroformed core has been designed and constructed. The design of the first electroformed core has been established, and its constuction, as well as that of a similar core having soldered joints for comparative study, was started.

Tensile test data on electroformed copper from a fluoborate bath produced at Savage Rowe Company averaged approximately 27,500 psi with a uniform elongation of 8.0%. The limited fatigue data available indicate a fatigue limit of 10,000 to 11,000 psi based on 10×10^6 cycles. Published data on the tensile strength of soldered joints vary from 13,000 to 29,000 psi with fatigue strengths of 200 to 400 psi for stresses to produce damage in 3,000,000 cycles. The published literature on the properties of electroformed copper give tensile strengths varying from 17,000 to 90,000 psi depending upon plating conditions. Grain size has a pronounced affect on the strength, the finer grained deposits being the stronger.

1. INTRODUCTION

This is a six month progress report covering research activities from Oct. 1, 1962 to April 1, 1963. Owing to the problems of the recruitment of personnel and the start of the fall semester at the University, essentially full-time studies began Oct. 1, 1962.

The research reported here involves a study of the feasibility of design and the performance characteristics of an air-water heat exchanger suitable for automotive application which is partially or wholly manufactured by the electroforming process. At present, common automobile radiator design and manufacture process consists of preformed tubes or water channels furnace soldered to dimpled or otherwise corrugated strip spacers forming a fairly compact and inexpensive matrix. Owing to the presence of the solder joints, however, there appears to be a definite possibility for design improvements if such joints can be eliminated. From the standpoint of thermal performance, the presence of solder is disadvantageous as it introduces undesirable thermal resistance at a critical point in the heat-flow path. This tends to require larger and heavier radiators to accomplish a given cooling task. Furthermore, soldered joints are subject to selective chemical attack from salt deposited on the highways to melt ice in the winter and to suppress dust in the summer. Such chemical attack causes further loss in thermal capacity by separating the spacer from the water channels as well as by providing a source for engine coolant leakage. Soldered joints are also susceptible to fatigue failures in service and the amount of solder necessary for manufacture adds undesirable weight to the radiator.

In view of these problems it has been proposed to study an entirely new method of forming the joints between the spacers (fins) and the water channels. This method is to produce an integral and metallurgically uniform joint either by electroforming both the spacer and water channel as a unit or by joining a preformed spacer and water channel by an electroforming process using copper as the material of construction. Either method, if successful, would produce a thermally superior joint and result in a radiator core of improved structural integrity and lower coolant leakage probability than the present soldered cores. The resulting core would probably be smaller, lighter, and more reliable than present automobile radiators. It is recognized that such a core must also be economically competitive. This latter consideration will probably be decided by the success of the electroforming process phase of this study in which it is expected that current techniques will require extension or that new ones will have to be developed based on an improved understanding of the mechanics of electroforming.

The research is divided between three related but parallel phases: (1) selection and evaluation of radiator core designs from the standpoint of their thermal and frictional pressure drop performance; (2) a metallurgical study of the physical properties of electroformed copper sheets and electroformed copper joints, including microstructure characteristics, and tensile and fatigue strengths; and (3) the production of an electroformed radiator satisfactory for automotive application. This last phase is being conducted by the Graham-Savage Associates, Kalamazoo, Michigan, under the direction of Mr. Frank K. Savage, Vice-President. Close technical liasson is maintained between the Graham-Savage Associates and The University of Michigan but contractual arrangements with the International Copper and Brass Research Association, Inc. are conducted independently. The first two phases of the research are being carried on at The University of Michigan with Prof. C. A. Siebert of the Department of Chemical and Metallurgical Engineering responsible for the metallurgical phase and Prof. R. B. Keller of the Department of Mechanical Engineering responsible for the radiator test program. Professor J. A. Clark of the Department of Mechanical Engineering is overall Project Director as well as having responsibility for the heat exchanger analysis and selection phase of the research. Mr. Richard D. Chapman, Director, Automotive Development, Copper and Brass Research Association, contributes to the general planning and assists in the coordination of the research between The University of Michigan, Graham-Savage and Associates, and the International Copper and Brass Research Association, Inc.

2. HEAT EXCHANGER ANALYSIS

The selection of the type of heat exchanger matrix suitable for an automotive radiator begins with an examination of the performance characteristics of typical existing air-water heat exchanger cores. The determination of the performance characteristics depends on the availability of generalized basic friction and heat transfer data of an experimental nature. Probably the most recent and comprehensive data of this kind presently available are those of Kays and London published in their book Compact Heat Exchangers.[1] This study reports the heat transfer and friction characteristics of 88 different kinds of extended surface heat exchangers suitable for gas turbine (gas-to-gas) or automotive (air-to-water) application. From this group 17 different matrices were selected for study and their relative thermal and friction performance determined. An eighteenth core included for comparison is a McCord Corporation type "GN" Honeycomb core for which the heat transfer and friction data has to be estimated from the best available source. A brief presentation of the analytical procedures follows.

The heat-transfer rate q in a heat exchanger may be expressed as follows

$$q = \epsilon(wc_p)_{min} (T_{h_i} - T_{c_i}) , \qquad (1)$$

in which ϵ is the heat transfer effectiveness.[1] The remaining symbols are defined in the nomenclature of this report. In this analysis the relative performance of air-water heat exchangers will be determined for the following conditions:

a. q is fixed
b. T_{h_i} is fixed
c. T_{c_i} is fixed
d. $(wc_p)_{min}$ is fixed
e. $(wc_p)_{max}$ is fixed.

For the usual automobile radiator $(wc_p)_{min}$ corresponds to the air-side and $(wc_p)_{max}$ corresponds to the water-side. The effectiveness ϵ is determined by the flow arrangement, i.e., counter flow, cross flow, etc., and the ratio $(wc_p)_{min}/(wc_p)_{max}$.[1] Hence, with the specifications a to e above, it is evident from Eq. (1) that ϵ will be fixed for all possible matrix shapes for a heat exchanger of a given flow arrangement. As shown by Kays and London[1] under these circumstances ϵ will then be a function only of the NTU, known as the number of transfer units in a heat exchanger. Furthermore, the NTU is defined as

$$NTU = \frac{UA}{(wc_p)_{min}} \quad . \tag{2}$$

Thus, we may now conclude that the relative performance of air-water heat exchangers may be determined on the basis of a fixed NTU which for the imposed restraints becomes

$$(UA)_1 = (UA)_2 \quad . \tag{3}$$

Now, if A is based on the air-side or finned-side of the exchanger, we have,

$$\frac{1}{UA} = \frac{1}{\eta_{oc} h_c A} + \frac{a}{A_w k} + \frac{1}{\eta_{oh} h_h A_h} \quad . \tag{4}$$

For the usual automobile radiator the last two terms in Eq. (4) are negligible, i.e., the air-side controls, so,

$$UA = \eta_{oc} h_c A \quad . \tag{5}$$

Dropping the subscript c as all symbols now refer to the air-side, we have from Eqs. (3) and (5)

$$(\eta_o h\ A)_1 = (\eta_o h\ A)_2 \tag{6}$$

where

η_o = total surface temperature effectiveness.

Hence, for purposes of comparison between various heat exchanger matrices at constant NTU, their relative volumes may be given as

$$\frac{V_1}{V_2} = \frac{(UA/V)_2}{(UA/V)_1} = \frac{[(\eta_o h)(A/V)]_2}{[(\eta_o h)(A/V)]_1} \quad . \tag{7}$$

A similar formulation may be written in which a "reference heat exchanger" matrix is used for comparison between all the others. Designating this reference exchanger by the subscript o we have,

$$\frac{V}{V_o} = \frac{[(\eta_o h)(A/V)]_o}{[(\eta_o h)(A/V)]} \quad . \tag{8}$$

With this formulation, then, any other two matrices, say 4 and 8 may be compared on a volume basis by

$$\frac{V_4}{V_8} = \frac{(V/V_o)_4}{(V/V_o)_8} \quad . \tag{9}$$

Now, the heat transfer parameter, the Stanton number, the flow parameter, the Reynolds number are defined as

$$St = \frac{h}{Gc_p} \tag{10}$$

$$Re = \frac{4r_h G}{\mu} \tag{11}$$

so,

$$\frac{h_o}{h} = \frac{St_o G_o}{St\ G} = \frac{(St_o)(w/A_c)_o}{(St)(w/A_c)} \quad , \tag{12}$$

which for constant air-side flow w, becomes,

$$\frac{h_o}{h} = \frac{St_o}{St} \cdot \frac{A_c}{A_{co}} \quad . \tag{13}$$

Because the air-side flow is the same in all comparisons, the Prandtl number is constant. Basic heat transfer data are given in terms of $St \cdot Pr^{1/3}$. Thus,

$$\frac{St_o}{St} = \frac{(St \cdot Pr^{2/3})_o}{St \cdot Pr^{2/3}} \quad .$$

Hence, from Eq. (8) we have for a fixed A_{FR}, the frontal area of the heat exchanger,

$$\frac{V}{V} = \frac{(\eta_o)_o}{(\eta_o)} \left(\frac{St_o}{St}\right) \left(\frac{A_c}{A_{co}}\right) \frac{(A/V)_o}{(A/V)}$$

$$= \frac{(\eta_o)_o}{(\eta_o)} \left(\frac{St_o}{St}\right) \frac{(A_c/A_{FR})}{(A_c/A_{FR})_o} \frac{(A/V)_o}{(A/V)}$$

$$= \frac{(\eta_o)_o}{(\eta_o)} \left(\frac{St_o}{St}\right) \left(\frac{\sigma}{\sigma_o}\right) \left(\frac{\alpha_o}{\alpha}\right) \tag{14}$$

where

$$\sigma \equiv \frac{A_c}{A_{FR}} , \tag{15}$$

$$\alpha = \frac{A}{V} = \beta\sigma \tag{16}$$

and

$$\beta = \frac{A}{V_B} .$$

Kays and London[1] report corresponding values of St, Re, σ, and α for the first 17 of the 18 heat exchanger surfaces considered in this report. Since the total volume of the matrix is written as $A_{FR} \cdot L$, where L is the depth of the matrix in the air flow direction, Eq. (14) may also be written for fixed frontal area and total surface temperature effectiveness, as

$$\frac{L}{L_o} = \left(\frac{St_o}{St}\right) \left(\frac{\sigma}{\sigma_o}\right) \left(\frac{\alpha_o}{\alpha}\right) = \frac{V}{V_o} . \tag{17}$$

The Reynolds number ratio is written for constant w and A_{FR} from Eq. (11) as

$$\frac{Re}{Re_o} = \frac{(r_h/r_{ho})}{(\sigma/\sigma_o)} . \tag{18}$$

For tube-fin matrices, σ is uniquely specified by the particular matrix under consideration. In the case of plate-fin designs the ratio σ depends on the thickness, δ of the water channel and is computed from

$$\sigma = \frac{1}{1+\delta/b} . \tag{19}$$

In these calculations δ is taken to be 0.080 in.

The above relationships permit the relative comparison between the heat transfer matrices from the standpoint of their thermal characteristics. A second important basis for comparison is the relative frictional pressure loss. Entrance and exit pressure losses are not included in this. The frictional pressure drop is expressed as

$$\Delta p = f \frac{L}{r_h} \frac{(w/A_c)^2}{2g_o\rho} = f \frac{L}{r_h} \frac{1}{A_c^2} \left(\frac{w^2}{2g_o\rho} \right) . \tag{20}$$

Hence, for the various matrices having constant frontal area, the relative frictional pressure loss is

$$\frac{\Delta p}{\Delta p_o} = \frac{(f/f_o)(L/L_o)}{(r_h/r_{ho})(\sigma/\sigma_o)} . \tag{21}$$

The last type of comparison to be made combines both the relative heat transfer and the relative friction. This is on the basis of heat transfer per unit volume per unit pressure drop. On this basis a favorable exchanger is one which has a large value of this parameter. Thus defining,

$$\psi = \frac{(q/V)}{\Delta p} , \tag{22}$$

we have the formulation of the relative value of this parameter as

$$\frac{\psi}{\psi_o} = \frac{(q/V)/\Delta p}{(q/V)_o/\Delta p_o}$$

$$= \frac{1}{(L/L_o)(\Delta p/\Delta p_o)} . \tag{23}$$

Equation (23) also may be regarded as the relative value of the heat transfer rate per unit volume to frictional pumping power corresponding to the condictions specified.

Comparison between the various matrices is made for the volume ratio (and depth ratio), Eq. (17), frictional pressure drop ratio, Eq. (21), and heat transfer per unit volume per unit frictional pressure drop ratio, Eq. (23). All are based on a reference heat exchanger for reference conditions, defined below.

The 18 matrices considered here consist of six tube-fins, nine plate-fins, two tube-banks and one Honeycomb type. The geometry and basic friction and heat transfer data of the first 17 are given in Figs. 1-17, taken from Kays and London.[1] The eighteenth is a McCord Corporation type "GN" Honeycomb replacement core having 1/4-in. square air passages, 2-1/4 in. long. Since basic heat transfer and friction data are not available for this matrix, its performance was estimated from data in Kays and London for a dimpled tube having approximately the same hydraulic diameter as the selected Honeycomb core.

2.1. REFERENCE HEAT EXCHANGER AND REFERENCE CONDITIONS

The reference heat exchanger is a plate-fin matrix having strip-fins and is the Kays and London surface designated as 1/8-15.2, indicating that it is made of 1/8 in. wide fins and has 15.2 fins/in. The width b of the air-flow channel is 0.414 in. In this report the reference heat exchanger is designated as surface 14 and its geometry and basic heat ransfer and friction characteristics are given in Fig. 14.

In order to have a specific flow condition for which all comparisons may be made, the following are taken

Air velocity = 10 ft/sec
Air temperature = 100°F
$\mu = 1.285 \times 10^{-5}$ lbm/ft/sec
$\rho = 0.071$ lbm/ft^3

Hence,

$$4r_{ho} = 0.1042 \text{ in.} = 0.00868 \text{ ft}$$

$$\sigma_o = 1/(1+0.080/0.414) = 0.838$$

$$\beta_o = 417 \text{ ft}^2/\text{ft}^3$$

$$\alpha_o = \beta_o\sigma_o = (417)(0.838) = 350$$

$$Re_o = 4r_{ho}G_o/\mu = 4r_{ho}(w/A_c)_o/\mu$$

$$= 4r_{ho}\rho VA_{FR}/\mu(\sigma_o A_{FR}) = 4r_{ho}/\sigma_o\ (\rho V/\mu)$$

$$= (0.00868)(0.071)(10)10^5/(0.838)(1.285)$$

$$= 572.$$

From Fig. 14 corresponding to $Re_o = 572$ we find,

$$(St\text{-}Pr^{2/3})_o = 0.0155 ,$$

and

$$f_o = 0.093 .$$

2.2. HEAT EXCHANGER MATRICES STUDIES

A summary of the 18 heat exchanger matrices selected for study is given in Table 1.

2.3. HEAT TRANSFER AND FRICTION DATA

The computed data for heat transfer and friction including the matrix parameters of σ, α, and β and their relative values are summarized in Tables 2 and 3.

2.4. RESULTS AND CONCLUSIONS

The relative volume or relative depth, V/V_o or L/L_o, relative friction pressure drop, $\Delta p/\Delta p_o$, and the relative heat transfer per unit volume per unit pressure drop, ψ/ψ_o are plotted in Figs. 18-20. From these results it is possible to compare all of the 18 matrices according to volume, pressure drop, and heat transfer per unit volume per unit pressure drop. As is evident by inspection, matrix 7 has lowest pressure drop but largest volume. From Table 1 it will be noted that this matrix is of the plate-fin type and very open with only 5.3 fins/in. and the second lowest area to volume ratio. The heat transfer per unit volume per unit pressure drop for this matrix is, however, rather poor, which is a result of its open design. From the standpoint of compactness matrix 12 is especially outstanding. This matrix has the smallest volume of them all (Fig. 18), and the highest heat transfer per unit volume per unit pressure drop (Fig. 20), although its frictional pressure drop is only moderately favorable (Fig. 19). The round tube banks (16 and 17) suffer from high pressure drop and high volume and consequently have very poor heat transfer per unit volume per unit pressure drop. The Honeycomb matrix, 18, also shows up poorly from the standpoint of compactness. Its pressure drop is second lowest but its heat transfer performance is not significant compared with the plate-fin designs.

These results indicate the superiority of the plate-fin type of matrix from the standpoint of maximum heat transfer per unit volume, minimum weight, and probably minimum cost. The benefit of turbulence promoters obtained by deforming the fins (wavy) is evident. The penalty is, of course, increased pressure drop but compactness is gained.

TABLE 1

Summary of Heat Exchanger Matrices*

Matrix No.	Classification	Matrix Type	Kays and London	Fins/in.	Hydraulic Diameter, in.	A/V ft^2/ft^3
1	Flat tubes, continuous fins	Flat tube, plain continuous fin	9.68-0.87	9.68	0.1416	229
2	Flat tubes, continuous fins	Flat tube, ruffled continuous fin	9.68-0.87R	9.68	0.1416	229
3	Flat tubes, continuous fins	Flat tube, plain continuous fin	9.1-0.737-S	9.1	0.1656	224
4	Flat tubes, continuous fins	Flat tube, ruffled continuous fin	9.29-0.737-SR	9.29	0.1622	228
5	Flat tubes, continuous fins	Flat tube, ruffled continuous fin	11.32-0.737-SR	11.32	0.1382	270
6	Round tube, continuous fins	Round tube, continuous fin	8.0-3/8T	8.0	0.1430	179
7	Plate fin, plain fins	Plain fin, b = 0.470 in.	5.3	5.3	0.2420	161
8	Plate fin, plain fins	Plain fin, b = 0.823 in.	9.03	9.03	0.1828	222
9	Plate fin, plain fins	Plain fin, b = 0.418 in.	15.08	15.08	0.1052	348
10	Plate fin, plain fins	Plain fin, b = 0.250 in.	19.86	19.86	0.0738	424
11	Plate fin, wavy fins	Wavy fin, b = 0.413 in.	11.44-3/8W	11.44	0.1272	294
12	Plate fin, wavy fins	Wavy fin, b = 0.413 in.	17.8-3/8W	17.8	0.0836	432
13	Plate fin, strip fin	Strip fin, b = 0.414 in.	3/32-12.22	12.22	0.1343	292
14	Plate fin, strip fin	Strip fin, b = 0.414 in.	1/8-15.2	15.2	0.1042	350
15	Plate fin, Louvered fin	Louvered fin b = 0.250 in.	14/-11.1	11.1	0.1214	278
16	Round tube bank	Staggered	S-1.50-1.25(S)	--	0.1980	80.3
17	Round tube bank	In-line	I-1.50-1.25(S)	--	0.1980	80.4
18	Honeycomb	1/4-in.-2-1/4 in.	---	--	0.1410	192

*Round tubes with circular fins not considered since for available basic heat transfer data, tubes are larger than 3/8-in. dia and area/volume ratio is less than 170. These would not complete with the above configurations.

TABLE 2

Heat Transfer Data

Matrix No.	$4r_h$	r_h/r_{ho}	σ	σ/σ_o	β	α	α/α_o	Re/Re_o	Re	$St \cdot Pr^{2/3}$	St/St_o	L/L_o
1	0.1416	1.36	0.697	0.833	229	229	0.655	1.635	935	0.0063	0.405	3.14
2	0.1416	1.36	0.697	0.833	229	229	0.655	1.635	935	0.0079	0.510	2.50
3	0.1656	1.59	0.788	0.941	224	224	0.640	1.690	967	0.0110	0.710	2.07
4	0.1622	1.55	0.788	0.941	228	228	0.654	1.65	945	0.0115	0.740	1.98
5	0.1382	1.33	0.780	0.930	270	270	0.771	1.43	820	0.0110	0.710	1.70
6	0.1430	1.37	0.534	0.637	179	179	0.511	2.15	1230	0.0095	0.611	2.04
7	0.242	2.32	0.855	1.02	188	161	0.460	2.28	1300	0.0059	0.380	5.83
8	0.1828	1.75	0.911	1.09	244	222	0.635	1.61	920	0.0061	0.384	4.48
9	0.1052	1.01	0.840	1.00	414	348	0.995	1.00	572	0.0085	0.547	1.83
10	0.0738	0.707	0.757	0.905	561	424	1.215	0.782	447	0.0110	0.710	1.05
11	0.1272	1.22	0.836	1.00	351	294	0.840	1.22	699	0.0170	1.10	1.07
12	0.0836	0.800	0.835	1.00	514	432	1.235	0.800	468	0.0172	1.11	0.730
13	0.1343	1.29	0.858	1.02	340	292	0.833	1.265	725	0.0175	1.13	1.090
14	0.1042	1	0.838	1	417	350	1	1	572	0.0155	1	1
15	0.1214	1.162	0.758	0.905	367	278	0.795	1.285	736	0.0140	0.905	1.26
16	0.1980	1.90	0.333	0.398	80.3	80.3	0.228	4.77	2730	0.0130	0.840	2.08
17	0.198	1.90	0.388	0.463	80.4	80.4	0.228	4.10	2350	0.0115	0.742	2.74
18	0.141	1.35	0.563	0.671	192	192	0.549	2.01	1150	0.00562	0.362	3.38

TABLE 3

Friction Data

Matrix No.	Re	f	f/f_o	L/L_o	r_h/r_{ho}	σ/σ_o	$\Delta p/\Delta p_o$	$\frac{L}{\Delta p}\left(\frac{\Delta p}{\Delta p_o}\right)$	ψ/ψ_o
1	935	0.023	0.247	3.14	1.36	0.833	0.685	2.15	0.465
2	935	0.035	0.377	2.50	1.36	0.833	0.832	2.08	0.480
3	967	0.036	0.387	2.07	1.59	0.941	0.535	1.108	0.904
4	945	0.042	0.452	1.98	1.55	0.941	0.614	1.218	0.822
5	820	0.042	0.452	1.70	1.33	0.930	0.621	1.056	0.946
6	1230	0.028	0.301	2.04	1.37	0.637	0.704	1.435	0.696
7	1300	0.016	0.172	5.83	2.32	1.02	0.423	2.465	0.405
8	920	0.023	0.247	4.48	1.75	1.09	0.633	2.835	0.353
9	572	0.036	0.387	1.83	1.01	1.00	0.705	1.290	0.775
10	447	0.041	0.441	1.05	0.707	0.905	0.725	0.741	1.350
11	699	0.092	0.990	1.07	1.22	1.00	0.869	0.930	1.075
12	468	0.083	0.893	0.730	0.800	1.00	0.815	0.595	1.680
13	725	0.100	1.075	1.090	1.29	1.02	0.891	0.971	1.030
14	572	0.093	1	1	1	1	1	1	1
15	736	0.070	0.753	1.26	1.162	0.905	0.900	1.135	0.880
16	2730	0.071	0.764	2.08	1.90	0.398	2.10	4.19	0.239
17	2350	0.053	0.570	2.74	1.90	0.463	1.78	4.88	0.205
18	1150	0.0125	0.1345	3.38	1.35	0.671	0.501	1.70	0.587

It was on the basis of these calculations that the matrix for the first electroformed model heat exchanger was selected. While matrix 12 is the most compact of the group it has a fairly high number of fins/inch—17.8. It was felt that for the first electroformed model the number of fins/inch ought not to exceed about 10 to reduce the electroforming problems and to have a design which is similar to current automotive practice. The model should however be of a plate-fin design with waviness in the fins, if possible.

2.5. FIRST ELECTROFORMED MODEL HEAT EXCHANGER

In view of the results of the study outlined above it was decided to construct the first electroformed radiator of a plate-fin design. To accomplish this in the most direct manner as quickly as possible, existing spacer stock deformed to provide waviness in the fins was obtained and a design established in which water channels would be electroformed at the fin roots. Mr. Richard D. Chapman secured the spacer stock. While it is recognized that such a design is not a completely electroformed heat exchanger, the critical points in the matrix, namely the joints, are electroformed. Undoubtably some development work will be necessary even to successfully accomplish this construction. When this is done, attention may then be given to more complete electroforming manufacture, should such appear desirable. When the spacer-water channel subassemblies are formed they will be soldered together and then joined to headers at each end. This design is shown in Fig. 21.

As a check on the thermal effectiveness of the electroformed joints in the first model, a second heat exchanger was planned which would be similar in all respects to the first except that the fins would be soldered to the water channels. The heat transfer performance of both exchangers would be determined experimentally in the test loop and wind tunnel.

3. RADIATOR HEAT TRANSFER PERFORMANCE TEST APPARATUS

3.1. INTRODUCTION

In order to determine experimentally the actual heat transfer performance of various radiator configurations, a heat transfer test loop was designed. Major emphasis was placed upon flexibility of operation: the capability for testing both scale models and full size automotive radiators over a range of vehicle speeds, air-side pressure drops, heat transfer rates, and heating water temperatures comparable to automotive application. The general configuration required to satisfy these requirements is shown schematically in Fig. 22 and consists of a heat transfer apparatus to supply a constant flow of water and heat transfer rate to the radiator, a wind tunnel to remove this heat from the radiator by a flow of cooling air through the radiator core at appropriate velocities and suitable instrumentation and controls.

3.2. HEAT TRANSFER APPARATUS

The heat transfer apparatus consists of a low-pressure steam supply used to heat the water, a bypass cooler, an accumulator, reservoir, pump, test radiator core controls, flow meter, and other instrumentation. The selection of water instead of steam as the hot-side heat transfer medium to the radiator was based on two considerations: first, water represents the fluid used in an automotive radiator; and second, the measurement of the heat transfer rate from water-wide temperature drop appeared to offer a convenient and reliable method for this determination. Radiator performance tests using steam are difficult to perform since the measurement of the heat transfer rate must be obtained by separating the liquid condensate flow from the vapor flow at the radiator exit. The principal problems associated with the use of water as the heat transfer medium is the accurate measurement of low temperature difference between the inlet and outlet water temperatures and the determination of precise adiabatic mixed mean temperatures at these points. These problems have been solved by using a thermopile at the inlet and outlet and a baffled flow mixer such that a true mixed mean temperature can be obtained.

Low-pressure steam is used in a shell and tube heat exchanger to heat the water in which the steam flow can be controlled either manually or automatically. The automatic controller takes the radiator water inlet thermocouple signal as an input and produces a pneumatic output signal to a pneumatically actuated control valve. A centrifugal pump is used to supply the pressure losses in the system. Control of the flow through the system is by means of a pump bypass, a pump discharge throttle valve, and a vernier bypass valve around the main control valve.

An accumulator is installed near the radiator inlet to maintain a given pressure level at the radiator inlet. An air regulator with constant bleed is used to pressurize the accumulator bag. The use of an accumulator to keep the water and the pressurizing gas separate permits the entire system to be free of entrapped air and also reduces the air dissolved into the water.

A bypass cooler in parallel with the test radiator permits the system to be operated without the test radiator or wind tunnel in the circuit. The bypass cooler may also be useful in stabilizing the system when tests are run at low mass flow rates and low heat transfer rates to the test radiator.

Copper lines and fittings are used throughout for ease of assembly and freedom from corrosion. Flexible hoses and swing joints are used to make radiator connections.

3.3. INSTRUMENTATION FOR HEAT TRANSFER APPARATUS

Water temperatures are measured by thermopiles (thermocouples connected in series) positioned in a flow-mixing baffle at both the radiator inlet and outlet stations to provide true mixed mean water temperatures. All temperatures will be continuously monitored and recorded on a self-balancing recording potentiometer.

Radiator inlet water pressure is measured with a bourdon tube gage, and radiator pressure drop with a manometer.

Water volume flow rate is measured with a rotameter. A turbine flow meter is provided for an independent check.

A typical set of automotive radiator performance conditions is given in Table 4 and may be compared with the design capabilities of the test loop shown in Table 5.

TABLE 4

Typical Maximum Automotive Radiator Performance

Water flow rate	300 lbm/min
Air flow rate	1760 ft^3/min
Air inlet temperature	94°F
Air outlet temperature	151°F
Water inlet temperature	184°F
Water outlet temperature	190°F
Heat transfer rate	1800 Btu/min

TABLE 5

Heat Transfer Loop Design Conditions

Heat transfer rate	100 hp or 4200 Btu/min
Water temperature in	190°F
Water temperature out	180°F
Water flow rate	50 gpm
Inlet water pressure	30 psia
Inlet steam temperature	350°F
Inlet steam pressure	50 psig

3.4. WIND TUNNEL

The wind tunnel consists of a contraction section, test section, diffuser, fan, and discharge ducting as shown in Fig. 23. The wind tunnel geometry and fan size were determined by the combination of the maximum simulated vehicle velocity, maximum radiator pressure loss, and maximum size of test radiator. The minimum operating conditions were determined by the minimum vehicle or inlet air velocity, and minimum test radiator size. These two limits, the maximum and minimum conditions, then provided the operating range and the flexibility requirements of the tunnel.

Three flow control methods were used to meet the air flow requirements of the tunnel: (1) a 2:1 fan speed reduction by means of switching the voltage of the electric motor which reduces fan air flow by this same ratio; (2) variable inlet guide vane geometry capable of producing a continuous variation in fan air flow from 15% to 100% of maximum air flow; and (3) a bypass around the test section which can produce a continuous variation in test section air flow from 10 to 100% of maximum test section air flow. The change in fan speed and the inlet guide vane geometry produce changes in fan characteristics while the tunnel bypass alters the total system flow characteristic to vary the test section air flow. The bypass also allows the fan to operate in a surge-free region at all times. The bypass is accomplished by constructing the contraction section and the test section as a single unit and then translating this unit forward relative to the fixed diffuser and fan. The bypass flow characteristic is shown in Fig. 24, and the combination of all three methods of flow control are shown in Fig. 25.

Exhaust air from the tunnel which is some 50°F above inlet or ambient air temperature is ducted downward through an opening in the second floor to the first floor area of the laboratory. This will eliminate the problems of re-ingestion of heated air and insure a nearly constant radiator inlet air temperature.

Photographs of the wind tunnel assembly, the test section region with removable, viewing, and access doors, and the bypass are shown in Figs. 26-28.

3.5. INSTRUMENTATION FOR WIND TUNNEL

A fairly elaborate pressure and temperature survey grid will be used for a detailed initial calibration and check-out. This unit will also be available for determination of local radiator performance. Final instrumentation after check-out will consist of eight total-static pressure tubes, four upstream, and four downstream and located so that the average flow conditions on both sides of the radiator.

The design conditions for which the wind tunnel is capable of meeting are given in Table 6.

TABLE 6

Wind Tunnel Design Conditions

Maximum radiator inlet velocity—equivalent to a vehicle speed of 100 mph	45 mph
Radiator pressure drop—at max tunnel velocity	5.1 in. H_2O
Total tunnel losses (incl radiator loss)	6.0 in. H_2O
Maximum radiator frontal dimensions	18 x 18 in.
Minimum radiator frontal dimensions	6 x 6 in.
Test section flow dimensions	24 x 24 in.
Inlet station of contraction section dimensions	72 x 72 in.
Fan volume flow rate (at 1580 rpm, 7 in. H_2O)	11,400 cfm
Fan drive motor, 440 V AC, 3 phase	25 hp

Construction and assembly of the basic wind tunnel was completed on April 1, 1963. The initial testing of its flow characteristics and the installation of the heat transfer loop and associated instrumentation is expected to be completed by the first part of May.

4. METALLURGICAL STUDIES

4.1. LITERATURE SURVEY OF SOLDERS

A limited literature survey was made to obtain selected data on the mechanical properties of solders and soldered joints. The properties included in this report are: tensile strength, shear strength, creep, and fatigue.

4.1.1. Tensile and Shear Strengths

Gonser and Heath[2] prepared tensile bars by casting solder into a split steel mold. The specimens were 7-5/16 in. long with a 2-in. parallel central section 3/8-in. in diam. The bars were annealed for 16 hr at 100°C. The tensile strengths were determined using a constant head speed of 0.5 in./min. The results are given in Table 7.

TABLE 7

Composition	Tensile Strength, psi
15% Sn, 0.25% Ag, 0.015% Bi, balance Pb	5,680
20% Sn, 0.25% Ag, 0.015% Bi, balance Pb	5,800
30% Sn, 0.25% Ag, 0.012% Bi, balance Pb	5,990
40% Sn, 0.25% Ag, 0.010% Bi, balance Pb	6,250
50% Sn, 0.25% Ag, 0.010% Bi, balance Pb	6,090
63% Sn, 0.25% Ag, 0.010% Bi, balance Pb	7,490

Thompson[3] prepared standard 0.505 test bars by casting solder into a split steel mold. The bars were tested in the as-cast condition using a head speed of 0.5 ipm. Their results are given in Table 8.

TABLE 8

Composition	Tensile Strength, psi
15% Sn, 85% Pb	5,270
20% Sn, 80% Pb	5,730
30% Sn, 70% Pb	6,810
40% Sn, 60% Pb	6,890
50% Sn, 50% Pb	6,400

Table 9 gives the results reported by Turkus and Smith.[4] They did not give the details of their tests.

TABLE 9

Composition	Tensile Strength, psi
20% Sn, 80% Pb	4,940
30% Sn, 70% Pb	5,390
40% Sn, 60% Pb	5,660
20% Sn, 2% Ag, 78% Pb	5,620
20% Sn, 1.5% Ag, 3% Bi, 74.85% Pb	8,120
30% Sn, 1% Ag, 69% Pb	8,810

Rhines and Anderson[5] prepared specimens by joining 0.75 in. copper rods which had been faced at the joining ends. A gap of 0.005 in. was used and the bars were heated to 60°C above the liquids of the solder, fluxed, soldered, and cooled. Their results are given in Table 10.

TABLE 10

Composition	Tensile Strength, psi
15% Sn, 85% Pb	13,300
33% Sn, 67% Pb	17,100
40% Sn, 60% Pb	14,100
50% Sn, 50% Pb	23,900
63% Sn, 37% Pb	29,000

Gonser and Heath[2] prepared lap joints using 70 copper, 30 zinc brass. Two methods of joining were used: (1) the closed method, i.e., maintaining a constant gap of 0.007 in.; and (2) the open method, i.e., the gap open to 0.030 in., solder applied, and then the gap closed to 0.007 in. Compensation was made for the offset character of the specimen and the head speed of the machine was 0.5 ipm. Their results are given in Table 11.

TABLE 11

Composition	Tensile Strength, psi	
	Open System	Closed System
15% Sn, 0.25% Ag, 0.015% Bi, balance Pb	4,265	4,050
20% Sn, 0.25% Ag, 0.015% Bi, balance Pb	4,490	4,880
30% Sn, 0.25% Ag, 0.012% Bi, balance Pb	5,450	4,790
40% Sn, 0.25% Ag, 0.010% Bi, balance Pb	5,550	5,250
50% Sn, 0.25% Ag, 0.010% Bi, balance Pb	5,750	5,240
63% Sn, 0.25% Ag, 0.010% Bi, Balance Pb	6,170	5,750

(Maximum value of each alloy was taken)

Turkus and Smith[4] results on lapped joints are given in Table 12. The details of their test procedure was not given.

TABLE 12

Composition	Tensile Strength, psi
20% Sn, 80% Pb	5,680
30% Sn, 70% Pb	5,770
40% Sn, 60% Pb	6,270
20% Sn, 2% Ag, 78% Pb	5,550
30% Sn, 1% Ag, 69% Pb	5,620

Gonser and Heath[2] performed shear tests on bulk solder samples. Their results are given in Table 13.

TABLE 13

Composition	Shear Strength, psi
15% Sn, 0.25% Ag, 0.015% Bi, balance Pb	4,470
20% Sn, 0.25% Ag, 0.015% Bi, balance Pb	4,740
30% Sn, 0.25% Ag, 0.012% Bi, balance Pb	5,500
40% Sn, 0.25% Ag, 0.010% Bi, balance Pb	5,680
50% Sn, 0.25% Ag, 0.010% Bi, balance Pb	5,870
63% Sn, 0.25% Ag, 0.010% Bi, balance Pb	6,060

Russell and Mack[6] reported the following shear strengths on bulk solder samples:

15% Sn, 85% Pb	4,280 psi
40% Sn, 60% Pb	4,900 psi

Rhines and Anderson[5] used butt soldered joints using 0.75 in. round copper bars which had been faced at the joining ends. The shear strengths were determined using a standard torsion test. Their results are given in Table 14.

TABLE 14

Composition	Shear Strength, psi
15% Sn, 85% Pb	5,640
33% Sn, 67% Pb	6,450
40% Sn, 60% Pb	8,280
50% Sn, 50% Pb	7,580
63% Sn, 37% Pb	8,000

4.1.2. Creep Properties

Baker[7] studied the creep properties of cast solders using specimen 0.564 in. in diam and 4 in. long in the parallel section. The results shown in Table 15 give the stress to produce a strain of 1×10^{-4} per day.

TABLE 15

Composition	At Room Temperature, psi	At 80°C, psi
30.4% Sn, balance Pb	115	39
49.5% Sn, balance Pb	125	28
62.2% Sn, balance Pb	335	68
40% Sn, 2.0% Sb, 0.10% Bi, 0.011% Ag, balance Pb	420	
60.2% Sn, 0.24% Sb, 0.015% Bi, 0.018% Ag, balance Pb	800	
62.2% Sn, 0.002% Bi, balance Pb	450	45
54.5% Sn, 3.6% Sb, 0.003% Bi, balance Pb	1,030	110

Baker[7] prepared lap joints using the "open method" described by Gonser and Heath[2] with a final gap of 0.006 in. The results reported in Table 16 are the 500-day stress-rupture strengths.

TABLE 16

40% Sn, 2% Sb, Balance Pb	At Room Temperature, psi	At 80°C, psi
For steel joints	325	120
For copper joints	390	120
For brass joints	470	120

4.1.3. Fatigue Properties

McKeown[8] conducted fatigue tests on lap joints. The fatigue machine was designed to apply alternating shear stresses to the specimen. Fatigue damage was determined by obtaining the decrease in tensile strength of a specimen after sustaining 3,000,000 cycles in the fatigue test. The results shown in Tables 17 and 18 give the maximum stress level which did not produce a decrease in the tensile strength. The mean stress used for the tests of Table 17 was 600 psi, and for the tests of Table 18 it was 900 psi.

TABLE 17

Composition	Maximum Alternating Stress, psi
63% Sn, balance Pb	400
50.4% Sn, balance Pb	400
31.5% Sn, balance Pb	360
18.9% Sn, balance Pb	350

TABLE 18

Composition	Maximum Alternating Stress, psi
63% Sn, 37% Pb	200
56% Sn, 3.2% Sb, balance Pb	310
30% Sn, 1.0% Sb, balance Pb	260

4.1.4. Summary

A limited literature survey on the mechanical properties of solders and soldered joints indicated tensile strengths of 5,000 to 8,000 psi for bulk solders and 13,000 to 29,000 psi on butt soldered joints depending on the composition of the solder. The fatigue strength of lap joint soldered interfaces was reported as 1000-1100 psi to produce damage in 3,000,000 cycles.

4.2. LITERATURE SURVEY OF THE MECHANICAL AND PHYSICAL PROPERTIES OF ELECTROFORMED COPPER

The majority of properties of electroformed copper have been determined on deposits from copper sulfate baths. The mechanical properties are either taken from standard tensile tests or from a hydraulic bulge test which is a modified Olsen cup ductility test.

The tensile strength of electrodeposited copper varies from 17,000 to 90,000 psi depending upon the plating conditions. In general the strength of the copper is related to the grain size and structure, being high for the finer grained copper deposits. There does not appear to be any correlation between the tensile strength and the hardness of the deposit, or the tensile strength and ductility as measured by percent elongation in the tensile test. Decreasing the bath temperature or increasing the current density appear to increase the tensile strength of the deposit, but specific additives to the bath in most cases have a greater effect on increasing the strength. Res-

idual stresses are usually low in electrodeposited copper. However, plating conditions are reported where the tension stresses have been found to be as high as 21,000 psi. The following summary of published papers gives specific details on the mechanical and physical properties of electrodeposited copper.

Bennett[9] deposited copper on a rotating cathode from a solution composed of 20% Cu SO_4-$5H_2O$ and 12% H_2SO_4. The cathode was an aluminum pipe 1 in. O.D. and 5.5 in. long. After the copper was deposited, the pipe was placed in a lathe and a section 1 in. wide and 2 in. from one end was turned down to a uniform thickness ranging from 0.040 to 0.060 in. The pipe was then cut into longitudinal sections in a milling machine, separated from the aluminum and pulled in an Olsen tensile testing machine. The strength reported was the average of five or more tests. The effect of speed of rotation, tempera ture of the bath, and current density are shown in Tables 19-21.

TABLE 19

Current density 500 amp/sq ft
Initial temperature 35°C

RPM	Tensile Strength, lb/sq in.
1,750	37,000
2,500	49,000
3,500	51,000
5,500	58,000

TABLE 20

Initial temperature 20°C
2,500 rpm

Amp/sq ft	Tensile Strength, lb/sq in.
300	60,000
400	68,000
510	40,000
1,100	35,000
1,700	14,000

TABLE 21

Initial temperature 50°C
5,500 rpm

Amp/sq ft	Tensile Strength, lb/sq in.
340	34,000
500	50,000
1,000	41,000
1,600	32,000
2,400	28,000
4,000	13,000

At a constant current density of 500 amps/sq ft, increasing the speed of rotation resulted in an increase of tensile strength. At constant speed of rotation, increasing the current density first results in an increase in strength, then reaches a maximum, and finally decreases. Variations in the bath composition has little, if any, affect on the strength of the deposite as shown in Table 22.

TABLE 22

5,500 rpm
Current density 500 amp/sq ft

% $CuSO_4 \cdot 5H_2O$	% H_2SO_4	Tensile Strength, lb/sq in.
12	15	60,000
20	15	58,000
25	15	55,000
15	12	60,000
15	25	57,000

Increasing the temperature from 25°C to 75°C has a pronounced affect on the strength as shown in Table 23.

TABLE 23

5,500 rpm
Current density amp/sq ft

Temp., °C	Tensile Strength, lb/sq in.
25	63,000
50	49,000
75	30,000

The author states that at current densities higher than 500 amps/sq ft no attempt was made to control the temperature of the bath, and it is his opinion that the decrease in strength at the high current densities noted in Tables 20 and 21 is due to an increase in temperature brought about by the plating conditions.

Sonoda[10] determined the strength of copper deposited as a sheet 120 cm x 30 cm and in varying thicknesses. The details of the electrodeposition process are not given. The author states that the properties varied from sheet to sheet, and even on sections of the same sheet. This is undoubtedly due to variations in thickness as he obtained the average thickness from weight measurements. The results are given in Table 24.

TABLE 24

Nominal Thickness, g/sq cm	Tensile Strength, kg/sq mm	Elongation, %
0.671	24.9	26
0.610	26.8	--
0.549	23.8	36
0.488	24.7	39
0.427	25.6	35
0.366	26.5	33
0.305	24.9	35

Shakespear[11] discussed the Anaconda commercial process for producing electrosheet copper and stated that the tensile strength varies from 30,000 to 40,000 psi, and elongation from 15 to 25%.

Altmeyer[12] reported a tensile strength of 39,000 psi and an elongation of 34%. These results are for copper deposited on a cathode, 68 cm in diam and 4 m long, rotating at 30-40 rpm.

Huessner, Balden, and Morse[13] discussed the effect of grain size and structures on the mechanical properties of electrodeposits. They include eight photomicrographs of copper deposited from baths of various compositions. Their mechanical property data are given in Table 25.

TABLE 25

Mechanical Properties of Acid Copper Deposits

Addition Agent	Tensile Strength, psi	Elongation % in 2 in.	Hardness V.H.N.
None	36,150	22	81
Molasses	33,000	21	81
Molasses and Thiourea	80,280	3	170

It can be seen that the addition of Thiourea to the bath produced a marked increase in the tensile strength and a marked decrease in ductility due to the fine grain structure resulting from the addition agent.

Prater and Read[14] used a hydraulic bulge test to determine the mechanical properties of copper. The bath consisted of 45 gm/l of copper and 200 gm/l of H_2SO_4. Glue was used as an addition agent. The sheet material was prepared by the Anaconda Process as described by Shakespear.[11] The average thickness was determined by weighing the test piece and calculating it, using 8.9 g/cc for the density of copper. Seven or more determinations were made for each thickness. The tensile strength of the 0.66 mil copper varied from 46,100 to 50,300 with an average of 48,000 psi. The dutility varied from 0.5 to 0.9%. The tensile strength of the 3.6 mil copper varied from 38,100 to 46,000 with an average of 41,000 psi. The ductility varied from 1.9 to 2.9%. It should be pointed out that the ductility measured in the bulge test are not related to ductility as measured in the tensile test.

Fedotev and Pozin[15] studied copper deposited from a bath containing 250 g/l $Cu\ SO_4 \cdot 5H_2O$, 50 g/l H_2SO_4, at a current density of 1 amp/sq dm and a temperature of 18°C. The cathode was a stainless steel plate 115 x 50 mm. Eight determinations were made for each thickness and the minimum, maximum, and average strengths are as follows:

Tensile Strength, psi

	Thickness		
	25μ	50μ	75μ
Minimum	28,400	29,800	30,700
Maximum	33,000	33,200	32,300
Average	31,200	31,600	31,400

Rochelle salt as a bath additive has the following affect on the tensile strength of the deposit.

Rochelle Salt, g/l	0	0.025	0.1	0.2	1.0	3.0	5.0
Tensile Strength, psi	33,500	12,100	12,100	11,900	8,050	1,690	1,240

Struyk and Carlson[16] determined the tensile strength of copper deposited from fluoborate baths of various compositions. The current density used was 300 amp/sq ft, and the thickness of the deposits was 0.020 in. Their results are given in Table 26. The deposit from a bath where the copper concentration is 120 g/l has a much higher tensile strength than one from a bath of 60 g/l of copper. However, the addition of 1.2 ml/l of molasses, or 2 g/l of Dacolyte to the 60 g/l copper bath resulted in producing deposits of comparable tensile strengths to those from the 120 g/l bath.

Such[17] indicates maximum tensile strengths of 43,000 psi and 60,000 psi may be obtained from Cyanide, and pyrophosphate baths respectively. However, the data are very meager and should be considered as only a rough approximation. Read and Whalen[18] studied the behavior of electroformed copper under alternating stresses. The copper was deposited from a bath containing 230 g/l Cu $SO_4 \cdot 5H_2O$, 50 g/l H_2SO_4 using a current density of 10 amp/sq ft. The specimens were not machined on the solution side of the specimen prior to testing in a Krouse bending fatigue machine. The thickness was 0.025 in. The tensile strength of the copper was 26,000 psi. Their results are given in Table 27. At a stress level of 9,500 psi there is a range of cycles to failure from 5.1×10^4 to 1.4×10^7. This is undoubtedly due to surface irregularites and possibly non-uniform thickness of the specimen.

Barklie and Davies[19] report a residual stress of essentially zero in copper deposited from a bath containing 200 g/l Cu $SO_4 \cdot 5H_2O$, 60 g/l H_2SO_4, when plated at 35°C and a current density of 30 amp/sq ft.

TABLE 26

Physical Properties of Deposits

Copper, g/l	Fluoboric Acid, g/l	Temp., °C		Yield Point, psi	Tensile Strength, psi	Elongation % in 2 in.	Rockwell, Hardness 15T
120	30	95		--	30,600	3.5	68-74
				--	22,500	2.5	
				28,000	34,500	3.5	
			Avg	28,000	32,500	3.2	
120	30	120		19,850	30,100	14.0	59-63
				19,200	29,100	14.0	
				21,750	29,400	15.5	
			Avg	20,230	29,500	14.5	
60	4	120		12,800	17,000	8.0	44-45
				13,200	17,200	7.5	
				12,700	15,700	6.5	
			Avg	12,900	17,100	7.3	
60*	4	120		22,600	30,800	11.0	64-70
				23,600	28,700	--	
			Avg	23,100	29,800	11.0	
60**	4	120		22,750	30,300	9.0	57-57.5
				(16,400)	(23,100)	(5.0)	
				20,200	30,300	12.0	
			Avg	21,480	30,300	10.5	

*With 1.2 ml/l molasses.
**With 2 g/l Dacolyte.

TABLE 27

Stress, psi	Cycles to Failure
10,800	3.9 x 10
10,800	3.3 x 10
10,800	6.6 x 10
9,500	5.4 x 10
9,500	4.2 x 10
9,500	5.1 x 10
9,500	1.1 x 10
9,500	4.0 x 10
9,500	3.0 x 10

Phillips and Clifton[20] reported residual stress measurements of copper deposited from various types of baths as shown in Table 28.

TABLE 28

Test No.	Type of Bath	Composition	pH	Temp., °F	C.D., asf
1	Acid copper	$CuSO_4$, 32 oz/gal H_2SO_4, 4 oz/gal	0.9	Room	30
2	Copper cyanide	NaCN, 9 oz/gal CuCN, 6 oz/gal Na_2CO_3, 2 oz/gal	12.8	125	15
3	Copper "K"	Recommended make-up	13.5	180	15
4	Copper "L"	Recommended make-up		140	15

Test No.	Thickness, in. (wt area/den)	Change of Deflection, in.	Calculated Stress,* psi	
			Steel Base	Bronze Base
1	0.0010	0.0002	1400	0
2	0.0005	0.0008	9900	7200
3	0.0005	0	0	
4	0.00154	0.0013	5200	

*The stress values are all positive or tension stresses.

Graham and Lloyd[21] determined stress values for copper deposited from alkaline cyanide baths. The standard bath consisted of 4 oz/gal copper, 0.8 oz/gal rochelle salt, and 4 oz/gal sodium carbonate to which a number of variables were introduced as shown in Table 29. It can be seen that the residual stress values vary from 15,400 psi in tension to 5,000 psi in compression.

TABLE 29

Test No.	Cathode Coefficient, %	Stress in Deposit, 1000 psi	Variable Studied
1	87.3	8.7	Standard
2	53.7	11.6	Current reversal
3	73.0	14.7	cd, 40 asf
4	82.5	11.5	Temperature 130°F
5	91.0	5.8	Temperature 180°F
6	95.0	6.4	No rochelle salt
7	78.1	9.0	Na CO , 9 oz/gal
8	86.0	9.0	Free NaCN, 1.6 oz/gal
9	87.0	8.6	NaOH to pH 13.0
10	88.4	9.7	Copper, 2.5 oz/gal
11	88.0	8.0	Copper, 5.0 oz/gal
12	88.0	8.4	CaCO , 100 ppm
13	86.1	8.6	K Fe(CN) , 0.5 g/l
14	85.2	8.8	K Fe(CN) , 1.0 g/l
15	87.2	11.3	Lead, 2 ppm
16	90.3	15.4	Lead, 75 ppm
17	90.0	- 4.0	KCNS, 2 oz/gal
18	95.3	- 4.7	KCNS, 2 oz/gal, no rochelle salt
19	98.5	3.1	A
20	98.9	3.6	A, lower pH
21	92.8	7.8	A, lower temperature
22	93.0	11.1	B
23	95.2	- 5.0	C
24	88.0	- 3.8	D

Fisher, Huhse, and Pawlek[22] studied the effect of gelatin additions on the residual stress in copper deposits. The bath was 1N $CuSO_4$ and 1N H_2SO_4. Increasing the gelatin content from zero to 0.1 g/l resulted in a gradual increase in the residual stress from approximately zero to 21,000 psi in tension. A further increase in gelatin content resulted in a gradual decrease in the residual stress, reaching zero at 0.2 g/l and a compressive stress of 1,400 psi at 0.25 g/l of gelatin.

Read and Graham[23] determined the elastic modulus of electro-deposited copper using the sonic technique. Thin wall tubes approximately 0.4 in. in diam and 4 to 6 in. long were prepared by plating on a steel mandrel coated with a thin layer of a low melting alloy. Their results are given in Table 30.

TABLE 30

Elastic Moduli of Cu Deposits Compared to Modulus for Drawn Cu Tubing $18.1 \pm 0.1 \times 10^6$ psi

Plating Bath	Current Density, asf	As-Plated Surface		Machined Surface	
		Elastic Modulus, psi x 10^6	Deviation from Ref, %	Elastic Modulus, psi x 10^6	Deviation from Ref, %
Purified acid Cu sulfate	10	13.9		16.2	
		13.9		16.1	
		14.0		16.0	
		14.2		16.1	
	(avg)	(14.0 ± 0.2)	22.7	(16.1 ± 0.1)	11.0
Impure acid Cu sulfate	10	15.7		17.1	
		15.8		16.9	
		16.2		16.9	
	(avg)	(15.9 ± 0.3)	12.2	(16.9 ± 0.1)	6.6
DuPont's P. R. Cu cyanide	40	16.1		16.8	
		16.0		16.9	
		15.8		16.8	
	(avg)	(15.9 ± 0.2)	12.2	(16.8 ± 0.1)	7.2

A considerable difference exists in the modulus value reported for the three different baths investigated in the as-plated condition, but not a very significant one on the machined surfaces. We may raise the question as to whether or not the differences noted in the as-plated condition are not due to non-uniform thickness, since thickness enters into the calculation of modulus when using the sonic technique for its measurement.

Hinnert and Krider[24] published the following expansion data for electrolytic copper:

Temperature Range, °C	Average Coefficient of Expansion, °C x 10^6
20- 60	16.6
20-100	16.8
20-200	17.3
20-300	17.7
20-400	17*

*From Esser and Eusterbrock, Archiv Eisenhuttenwesen, 14 (1941), 341.

4.2.1. Summary

Tensile strength data on electroformed copper reported in the literature vary from 17,000 to 90,000 psi. The strength is a function of the bath composition and plating conditions. The hardness of the plate does not have any correlation with the strength or ductility of the plate. In general, reducing the temperature or increasing the current density increases the strength of the copper. This is probably related to the fact that the grain size of the copper is decreased, which increases the strength.

4.3. TENSILE AND FATIGUE TEST ON ELECTROFORMED COPPER

Tensile tests were performed on copper which had been electroformed at the Savage Rowe Company in Kalamazoo. It is our understanding that the copper was deposited under the following conditions:

Temperature: 115°F
Current Density: 100 amp/sq ft
Agitation: Air
Bath Composition:

Copper fluoborate	443 g/l
Copper metal	120 g/l
Free fluoboric acid	45 g/l
Additives	None

The test samples were standard 0.5 in. wide strips and were run on an Instron self-aligning machine. The fracturing of the specimens occurred in an irregular manner in that part of the fracture appeared to be brittle and part of it appeared to be ductile. The ductility as measured on a fractured specimen was erratic due to the nature of the fracture. It was therefore decided to use "uniform elongation" as a measure of ductility, i.e., the percentage of elongation in two inches at the point where the test specimen reaches the maximum load.

The tensile tests on the first shipment of copper in December, 1962, indicated a wide scatter in the strength ranging from 30,000 to 39,000 psi. The results of the tensile test on the second shipment of copper in January, 1963, are somewhat lower but more uniform than the results on the first shipment of copper. Since fatigue tests are being run on the second shipment of copper, only the tensile test results on this shipment of copper are included in this report. They are somewhat lower than the values obtained on the first shipment of copper and no explanation has been found for this difference since the plating conditions were supposedly the same.

The thickness of the sheet material supplied varied from one end of the sheet to the other by as much as 0.007 in. The variation in thickness of a 2-in. gage length was as much as 0.003 in. However the point of fracture was not always at the point of minimum thickness. Therefore a thickness gradient was determined for each test piece and the cross-sectional area was computed at the point of fracture. The results of the tensile test are:

Specimen No.	Thickness, in.		Tensile Strength, psi	Uniform Elongation % in 2 in.
F1	0.0249		27,550	7.8
F2	0.0260		27,690	7.8
F3	0.0265		27,470	7.8
F4	0.0269		26,915	7.0
F5	0.0263		26,995	8.2
		Avg	27,324	7.7
G2	0.0106		27,735	9.0
G3	0.0109		26,970	8.2
G4	0.0118		28,475	11.0
G5	0.0131		28,090	7.3
		Avg	27,818	9.0

The microstructure of the copper is shown in Figs. 29-32. The specimens for microscopic examination were taken from the tensile test bars. The microstructure is a typical columnar structure of electro-deposited metals from baths that do not contain addition agents to produce a fine grain structure.

It was originally intended to use a Sonntag constant-load fatigue-testing machine to evaluate the properties of the electroformed copper under alternating stresses. However the design of the machine did not permit the use of loads below two pounds and the stress levels needed required loads of 0.5 pounds or less. It was therefore decided to use a constant deflection testing

machine, and this caused a few weeks delay in starting the fatigue program as it was necessary to obtain a Krouse testing machine, which is shown in Fig. 33. This machine was purchased from funds supplied by the University and made available to this research at no cost.

The thickness of the electroformed copper varied over the length and width of the test specimen. The range in variation of thickness was from a few ten thousandths to almost two thousandths of an inch. The average thickness was used in computing the load necessary to produce a given stress in the test specimen. The Krouse machine is designed to permit a desired weight to be suspended from the crank end of the specimen and electrical contact established at the deflection produced by the weight. The specimen is then attached to the crank and the eccentric on the crank adjusted until electrical contact is again established, which indicates that the specimen is again deflected to the same extent as it was when the weight was employed. This procedure eliminates the necessity of having to know the modulus of elasticity of the material. Variations in thickness, surface condition, etc., enhance the scatter that is normally encountered in fatigue test results. The data obtained to date cycling around zero mean stress are as follows:

Specimen No.	Average Thickness, in.	Stress, psi	Number of Cycles to Failure
4	0.020	12,000	10×10^6*
33	0.024	12,000	1.28×10^6
6	0.024	12,000	1.06×10^6
5	0.021	12,000	0.54×10^6
2	0.024	11,500	1.6×10^6
3	0.025	11,500	$0.9 - 2.2 \times 10^6$**
7	0.023	11,000	9.8×10^6
9	0.022	11,000	4.9×10^6
18	0.021	11,000	10×10^6
13	0.026	11,000	5.4×10^6
1	0.026	10,000	12×10^6

*Did not fail.

**Broke during night. Machine did not shut off.

From the limited data available it would appear that the endurance limit of this electroformed copper is somewhere between 10,000 and 11,000 psi.

REFERENCES

1. W. M. Kays and A. L. London, Compact Heat Exchangers, The National Press, Palo Alto, Calif., 1955.

2. B. W. Gonser and C. M. Heath, "Physical Properties of Soft Solders and the Strength of Soldered Joints," AIME Transactions, 122, p. 349 (1936).

3. J. G. Thompson, "Properties of Lead-Bismuth, Lead-Tin, Type Metal and Fusible Alloys," U.S. Bureau of Standards, Journal of Research, 5, p. 1085 (1930).

4. S. Turkus and A. A. Smith, Jr., "Low Tin Solders Containing Silver and Bismuth," Metals and Alloys, 15, p. 412 (1942).

5. F. N. Rhines and W. A. Anderson, "Substitute Solders," Metals and Alloys, 14, p. 704 (1941).

6. J. B. Russell and J. O. Mack, "Substitute Solders of the 15-85 Tin-Lead Type," AIME Transactions, 161, p. 382 (1945).

7. W. A. Baker, "The Creep Properties of Soft Solders and Soft Soldered Joints," Journal of Inst. of Metals, No. 2, p. 277 (1939).

8. M. McKeown, "Properties of Soft Solders and Soldered Joints British Non-Ferrous Research Association, Research Mograph, No. 5, p. 57 (1947).

9. C. W. Bennett, "Tensile Strength of Electrolytic Copper On a Rotating Cathode," Transactions, Am. Electrochemical Soc., 21, p. 245-274 (1912).

10. S. Sonoda, "The Properties of Sheets Deposited on Rotating Cathode," Transactions, Am. Electrochemical Soc., 52 (1927), p. 233-247.

11. W. H. Shakespear, "Development and Use of Anaconda Electro-Sheet Copper," AIME Transactions, 106, p. 441-448 (1933).

12. M. Altmeyer, "Manufacture of Sheets of Electrolytic Copper," Original in CUIVRE ET LAITON, 7 (1934), p. 367-370. Chemical Abstracts, 28, 6640.

13. C. E. Huessner, A. R. Balden, L. M. Morse, "Some Metallurgical Aspects of Electrodeposits," PLATING, 35, p. 554-557, 719-723, 768 (1948).

14. T. A. Prater and H. J. Read, "The Strength and Ductility of Electrodeposited Metals," PLATING, 36, p. 1221-1226 (1949). Ibidem, 37, p. 830-834, 850 (1950).

15. N. P. Fedotev and Iu. M. Pozin, "Effect of Surface-Active Substances on the Mechanical Properties of Electrolytic Deposits," J. of Appl. Chem. of the USSR, 31, p. 406 (1958).

16. C. Sruyk and A. E. Carlston, "Copper Plating from Fluoborate Solutions," Monthly Review of Electroplaters' Soc., 33, p. 932-934 (1946).

17. T. E. Such, "The Physical Properties of Electrodeposited Metals," METALLURGIA, 56, p. 61-66 (1957).

18. H. J. Read and T. J. Whalen, "The Ductility of Plated Coatings," Proceedings, Am. Electroplaters' Soc., 46, p. 318 (1959).

19. R. H. Barklie and H. J. Davies, "The Effect of Surface Conditions and Electrodeposited Metals on the Resistance of Materials to Repeated Stresses," Proceedings, Inst. of Machanical Engineers (London), 1, p. 731-750 (1930).

20. W. M. Phillips and F. L. Clifton, "Stress in Electrodeposited Nickel," Proceedings, Am. Electroplaters' Soc., 34, p. 97-110 (1947).

21. A. K. Graham and R. Lloyd, "Stress Data on Copper Deposits From Alkaline Baths," PLATING, 35, p. 449-450, 506 (1958).

22. H. Fishcer, P. Huhse, and F. Pawlek, "Internal Stress in Electrodeposited Copper," Zeitschrift fur Metallkunde, 47, p. 43-49 (1956).

23. H. J. Read and A. H. Graham, "The Elastic Modulus and Internal Friction of Electrodeposited Copper," Electrochemical Soc. Journal, 108, p. 73 (1961).

24. P. Hinnert and H. S. Krider, "Thermal Expansion of Some Copper Alloys," Journal of Research, National Bureau of Standards, 39, p. 419 (1947).

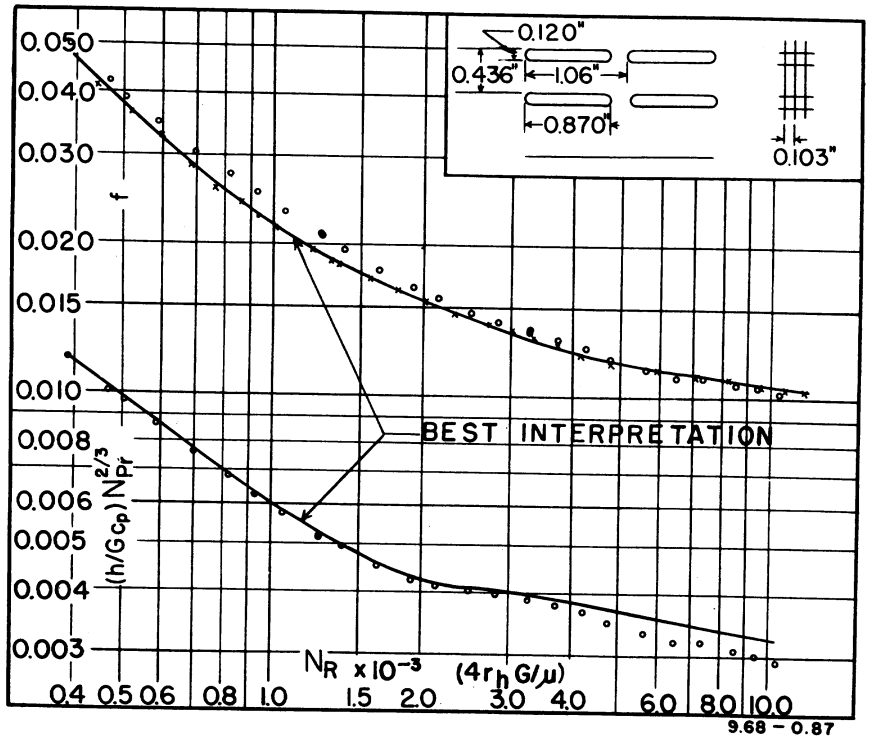

Fig. 1.

FINNED FLAT TUBES
SURFACE 9.68 – 0.87

Fin pitch – 9.68 per inch
Flow passage hydraulic diameter – $4r_h$=0.01180 ft.
Fin metal thickness – 0.004in.
Free-flow area/frontal area – σ=0.697
Total heat transfer area/total volume –α=229 $ft.^2/ft.^3$
Fin area/total area – 0.795

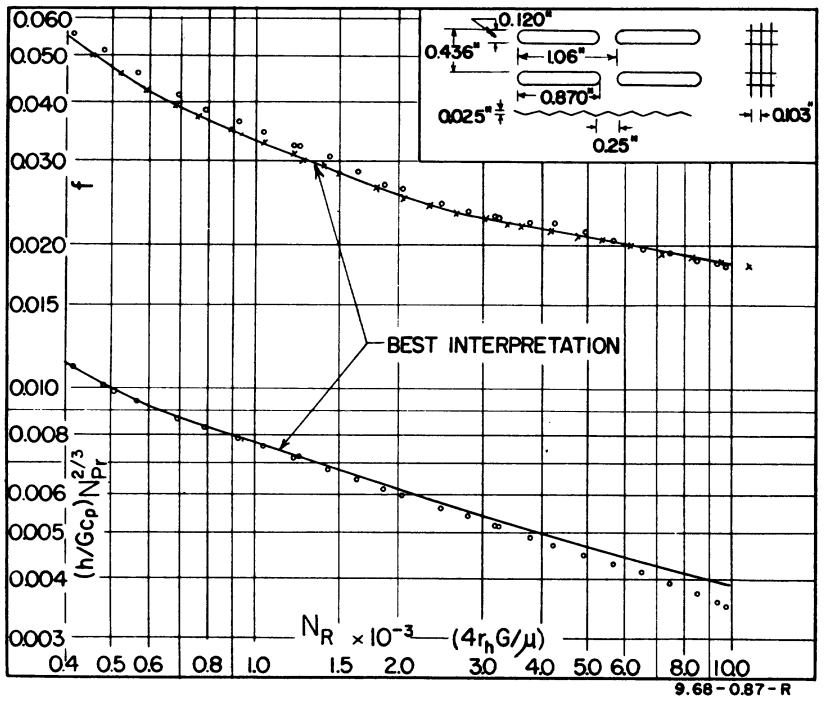

Fig. 2.

FINNED FLAT TUBES
SURFACE 9.68 – 0.87 – R

Fin pitch – 9.68 per inch
Flow passage hydraulic diameter – $4r_h$=0.01180 ft.
Fin metal thickness – 0.004 in.
Free-flow area/frontal area – σ=0.697
Total heat transfer area/total volume –α=229 $ft.^2/ft.^3$
Fin area/total area – 0.795

W. M. Kays and A. L. London, Compact Heat Exchangers, The National Press, Palo Alto, Calif., 1955 (reproduced by permission).

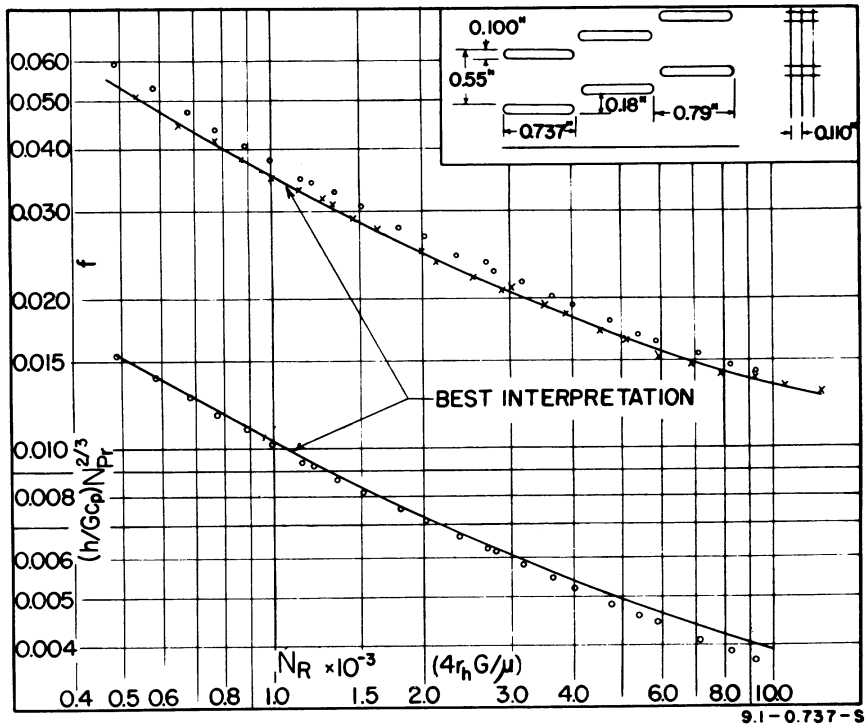

Fig. 3.

FINNED FLAT TUBES
SURFACE 9.1 - 0.737 - S

Fin pitch - 9.1 per inch
Flow passage hydraulic diameter - $4r_h$=0.01380 ft.
Fin metal thickness - 0.004 in.
Free-flow area/frontal area - σ =0.788
Total heat transfer area/total volume - α=224 $ft.^2/ft.^3$
Fin area/total area - 0.813

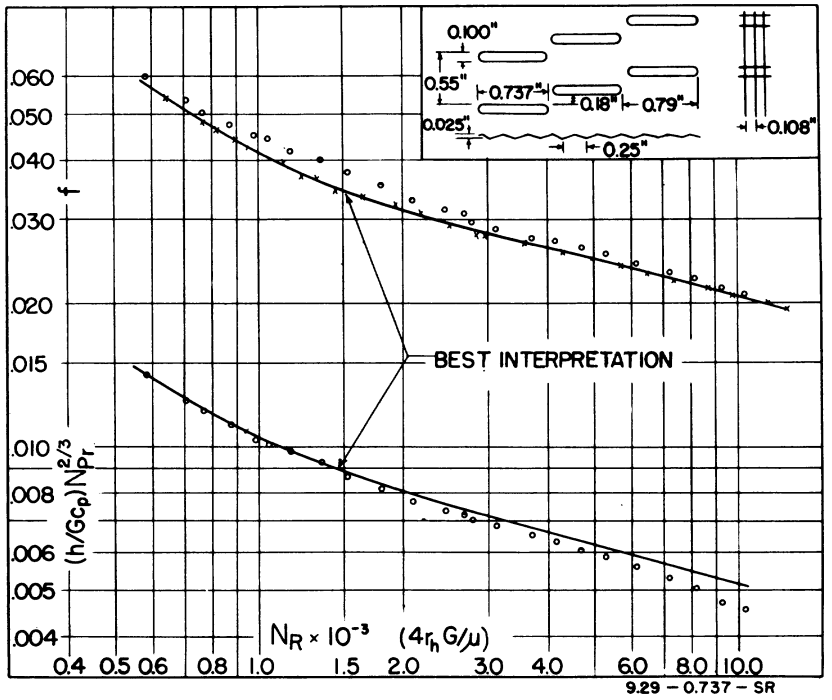

Fig. 4.

FINNED FLAT TUBES
SURFACE 9.29 - 0.737 -SR

Fin pitch - 9.29 per inch
Flow passage hydraulic diameter - $4r_h$=0.01352 ft.
Fin metal thickness - 0.004 in.
Free-flow area/frontal area - σ =0.788
Total heat transfer area/total volume - α=228 $ft.^2/ft.^3$
Fin area/total area - 0.814

W. M. Kays and A. L. London, Compact Heat Exchangers, The National Press, Palo Alto, Calif., 1955 (reproduced by permission).

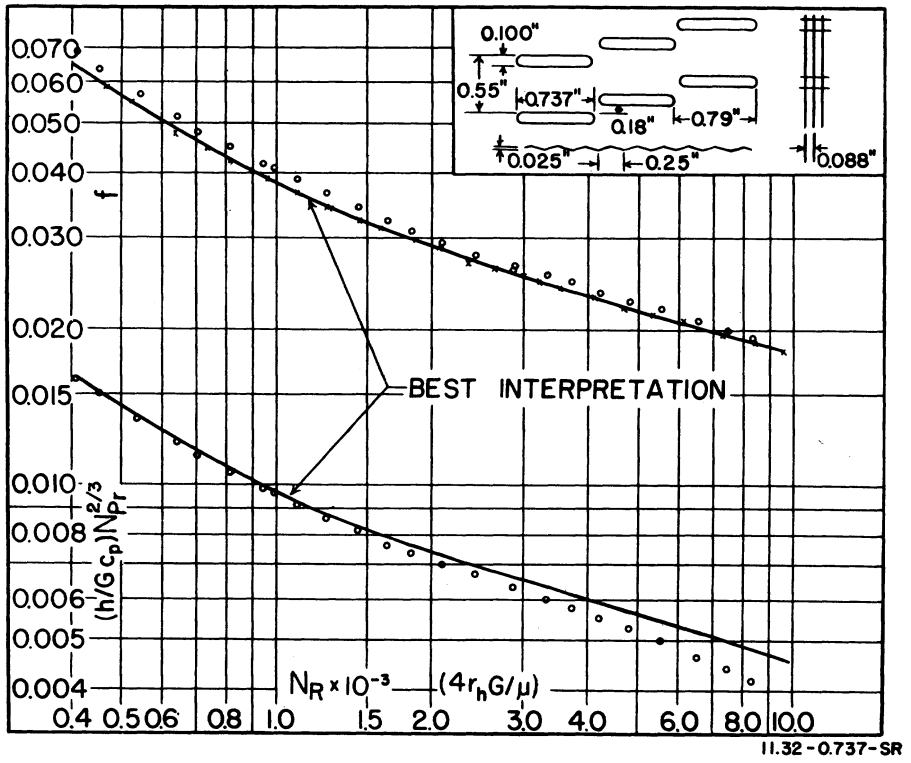

Fig. 5.

FINNED FLAT TUBES
SURFACE 11.32 - 0.737-SR

Fin pitch - 11.32 per inch
Flow passage hydraulic diameter - $4r_h$=0.01152 ft.
Fin metal thickness - 0.004 in.
Free-flow area/frontal area - σ =0.780
Total heat transfer area/total volume - α=270 $ft.^2/ft.^3$
Fin area/total area - 0.845

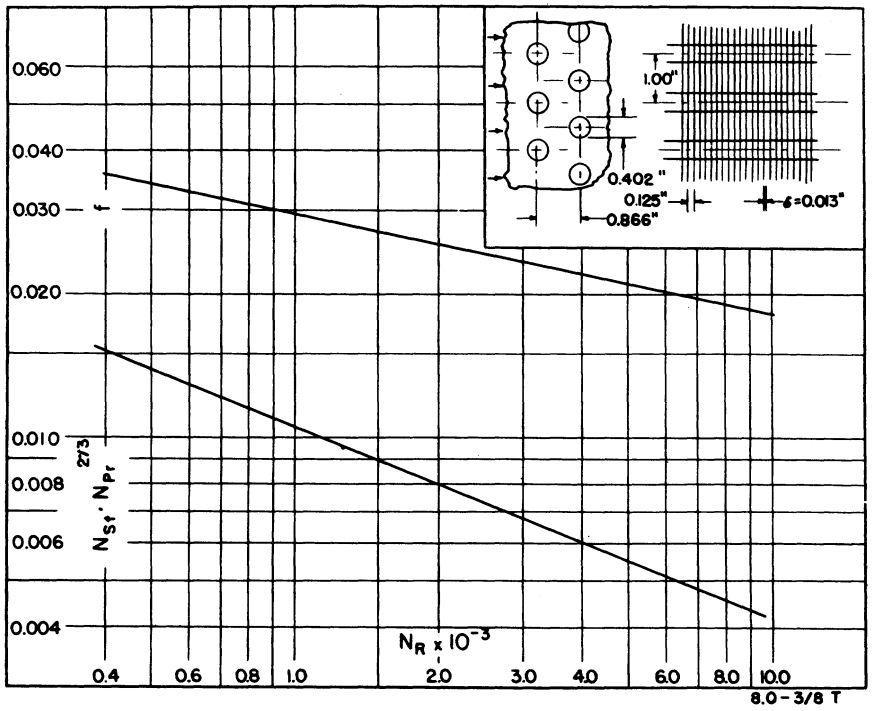

Fig. 6.

FINNED CIRCULAR TUBES
SURFACE 8.0 - 3/8 T
(Data of Trane Co.)

Tube outside diameter - 0.402 in.
Fin pitch - 8.0 per inch
Flow passage hydraulic diameter - $4r_h$=0.01192 ft.
Fin thickness - 0.013 in.
Free-flow area/frontal area - σ =0.534
Heat transfer area/total volume - α =179 $ft.^2/ft.^3$
Fin area/total area - 0.839

Note: Minimum free-flow area in spaces transverse to flow.
These data are included in this compilation because they apply to a compact surface configuration of considerable technical interest for which no data have been obtained on this project.

W. M. Kays and A. L. London, Compact Heat Exchangers, The National Press, Palo Alto, Calif., 1955 (reproduced by permission).

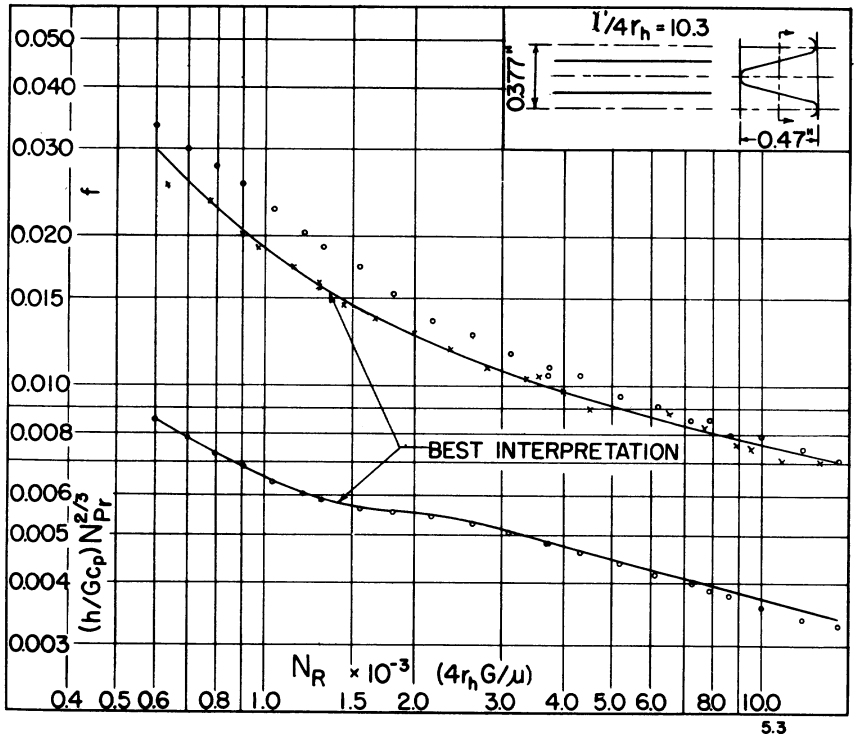

Fig. 7.

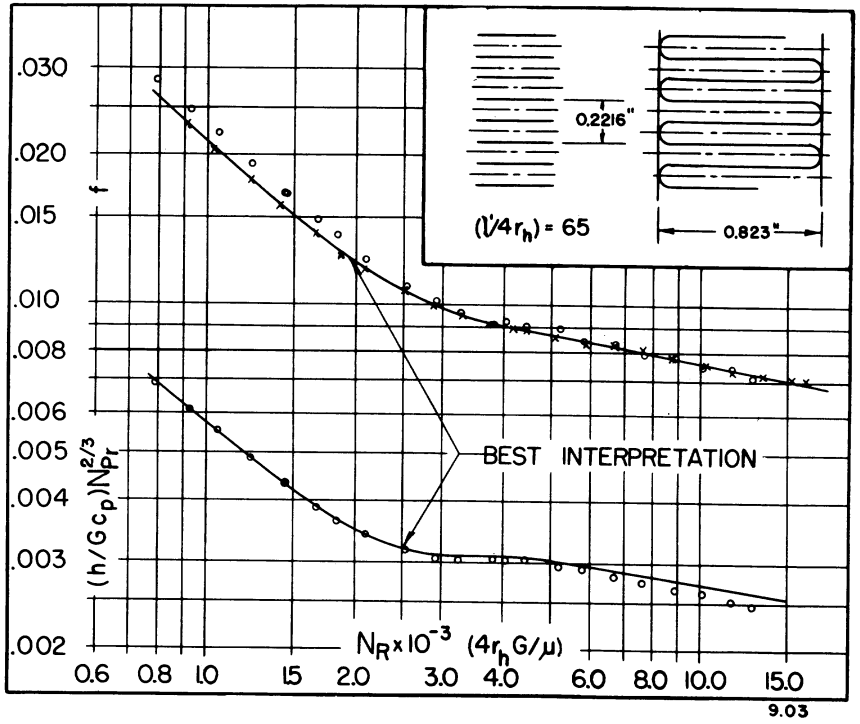

Fig. 8.

PLAIN PLATE-FIN
SURFACE 5.3

Fin Pitch - 5.3 per inch
Plate spacing - b=0.470 in.
Flow passage hydraulic diameter - $4r_h$=0.02016 ft.
Fin metal thickness - 0.006 in.
Total transfer area/volume between plates - β=188ft.^{2}/ft.^{3}
Fin area/total area - 0.719
$(l'/4r_h)$=10.3

PLAIN PLATE-FIN
SURFACE 9.03

Fin pitch - 9.03 per inch
Plate spacing - b=0.823 in.
Flow passage hydraulic diameter - $4r_h$=0.01582 ft.
Fin metal thickness - 0.008 in.
Total transfer area/volume between plates - β=244 ft.^{2}/ft.^{3}
Fin area/total area - 0.886
$(l'/4r_h)$=65

W. M. Kays and A. L. London, Compact Heat Exchangers, The National Press, Palo Alto, Calif., 1955 (reproduced by permission).

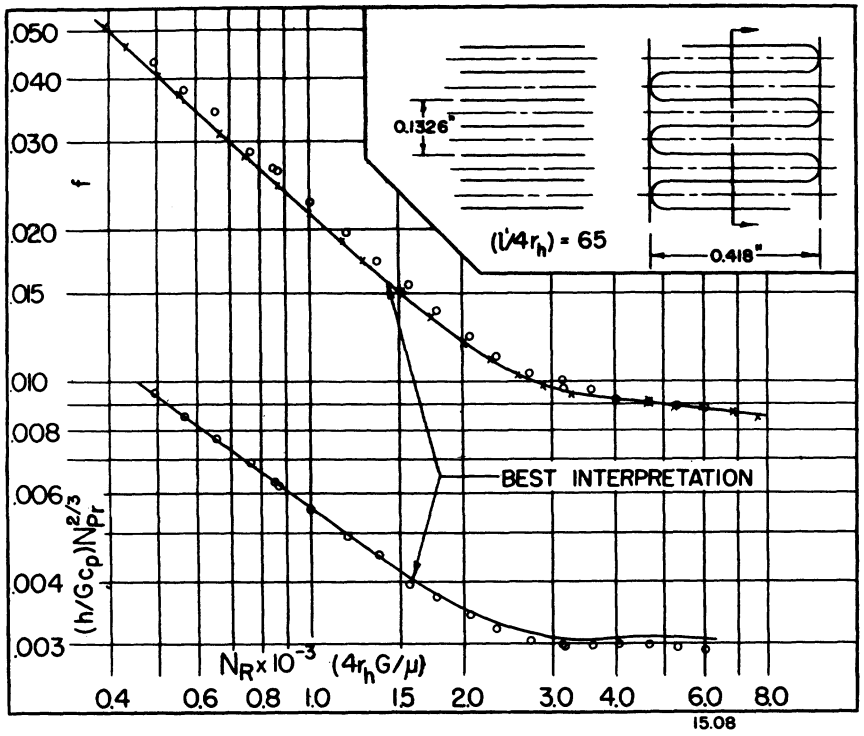

Fig. 9.

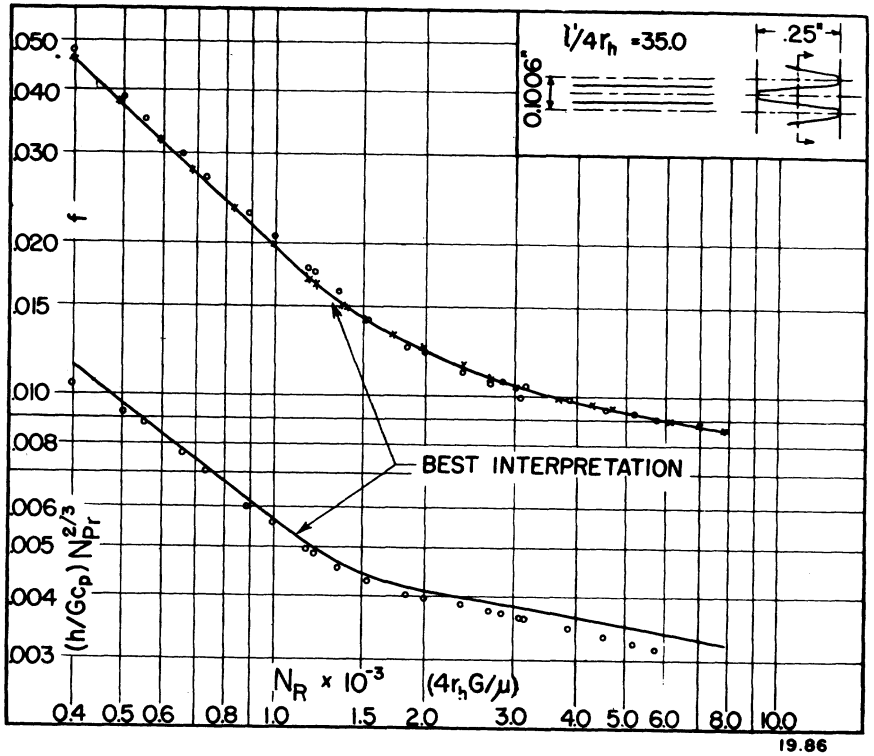

Fig. 10.

PLAIN PLATE FIN
SURFACE 15.08

Fin pitch - 15.08 per inch
Plate spacing - b=0.418 in.
Flow passage hydraulic diameter - $4r_h$=0.00876 ft.
Fin metal thickness - 0.006 in.
Total transfer area/volume between plates - β=414 $ft.^2/ft.^3$
Fin area/total area - 0.870
$(l'/4r_h)$=65

PLAIN PLATE FIN
SURFACE 19.86

Fin pitch - 19.86 per inch
Plate spacing - b=0.250 in.
Flow passage hydraulic diameter - $4r_h$=0.00615 ft.
Fin metal thickness - 0.006 in.
Total transfer area/volume between plates - β=561 $ft.^2/ft.^3$
Fin area/total area - 0.849
$(l'/4r_h)$=35.0

W. M. Kays and A. L. London, Compact Heat Exchangers, The National Press, Palo Alto, Calif., 1955 (reproduced by permission).

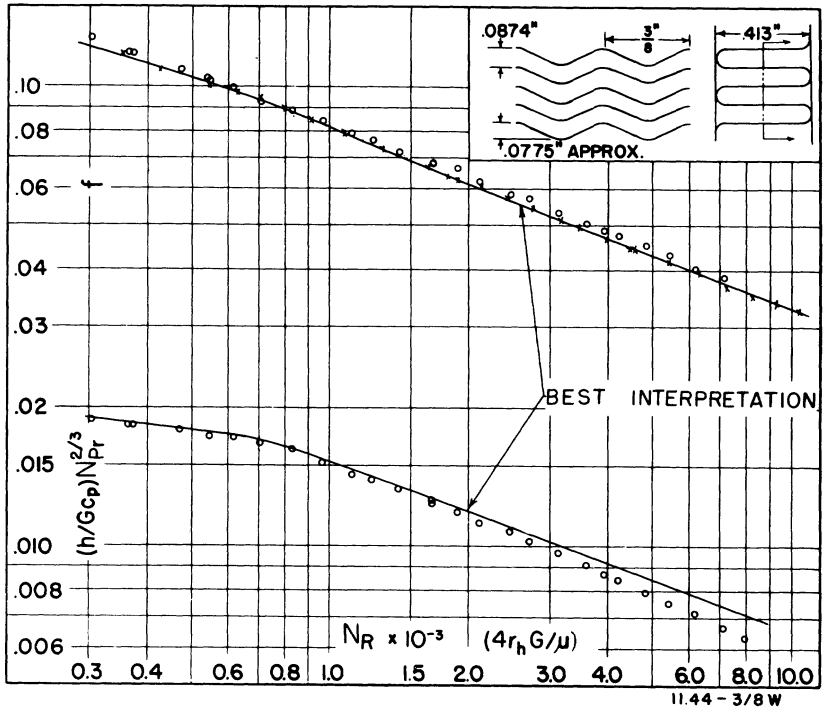

Fig. 11.

WAVY-FIN PLATE-FIN
SURFACE 11.44 - 3/8W

Fin pitch - 11.44 per inch
Plate spacing - b=0.413 in.
Flow passage hydraulic diameter - $4r_h$=0.01060 ft.
Fin metal thickness - 0.006 in.
Total heat transfer area/volume between plates - β =351 $ft.^2/ft.^3$
Fin area /total area - 0.847

Note: Hydraulic diameter based on free-flow area normal to mean flow direction.

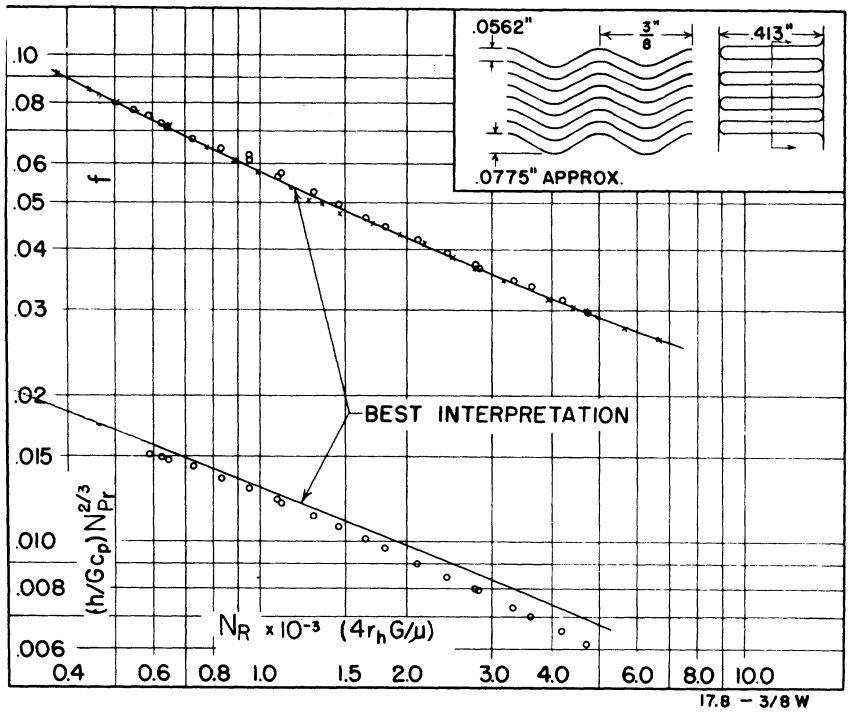

Fig. 12

WAVY-FIN PLATE-FIN
SURFACE 17.8 - 3/8W

Fin pitch - 17.8 per inch.
Plate spacing - b=0.413 in.
Flow passage hydraulic diameter - $4r_h$=0.00696 ft.
Fin metal thickness - 0.006 in.
Total heat transfer area/volume between plates - β =514 $ft.^2/ft.^3$
Fin area/total area - 0.892

Note: Hydraulic diameter based on free-flow area normal to mean flow direction.

W. M. Kays and A. L. London, Compact Heat Exchangers, The National Press, Palo Alto, Calif., 1955 (reproduced by permission).

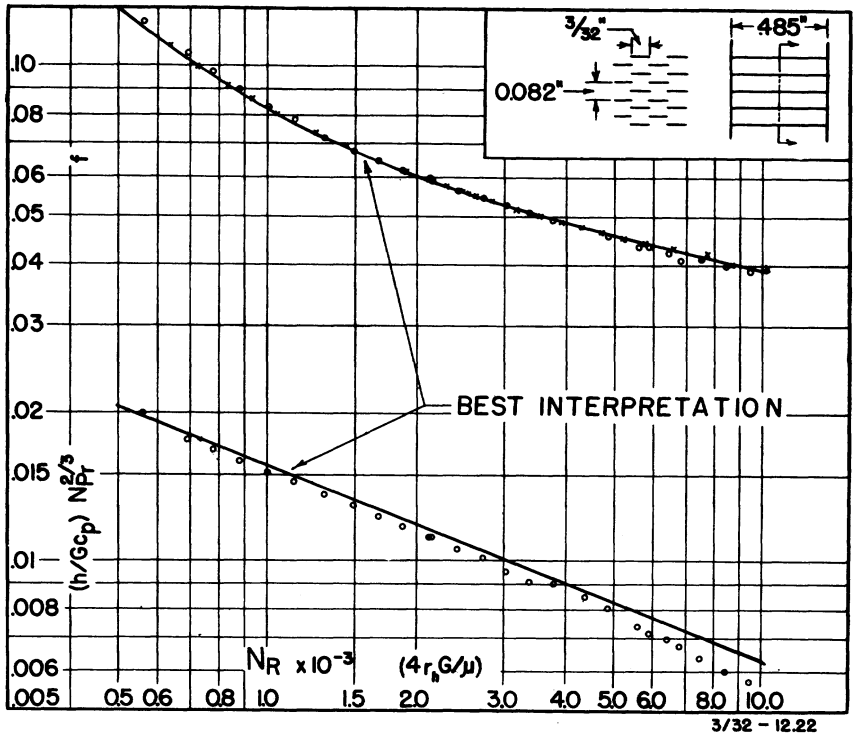

Fig. 13.

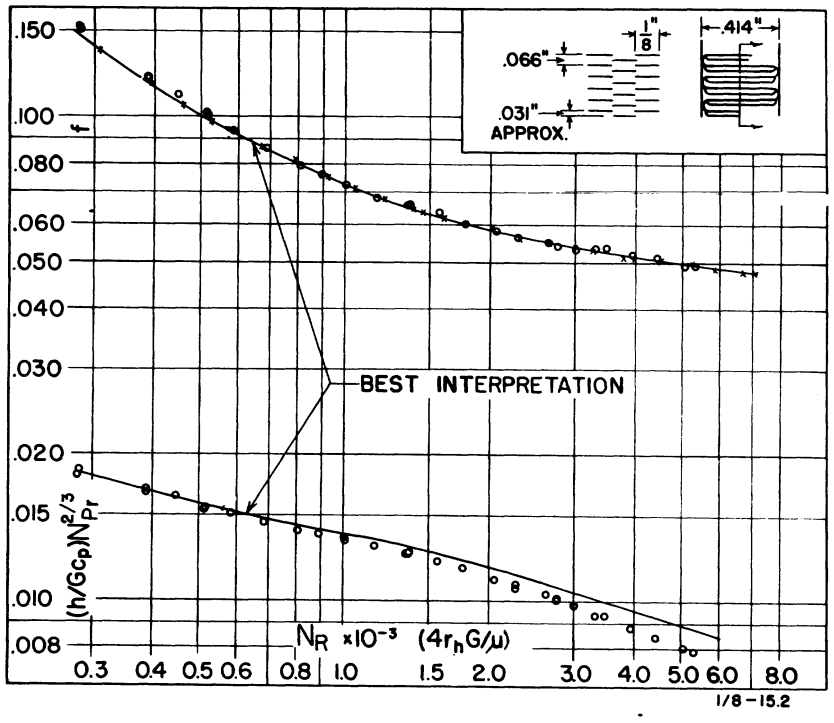

Fig. 14.

STRIP-FIN PLATE-FIN
SURFACE 3/32 - 12.22

Fin pitch - 12.22 per inch
Plate spacing - b=0.485 in.
Fin length - 0.094 in.
Fins staggered symmetrically
Flow passage hydraulic diameter - $4r_h$=0.01120 ft.
Fin metal thickness - 0.004 in.
Total heat transfer area/volume between plates - β=340 ft.^{2}/ft.^{3}
Fin area/total area - 0.862

Note: Fin leading and trailing edges slightly scarfed from fin cutting operation. Friction factors may be lower with clean fins.

STRIP-FIN PLATE-FIN
SURFACE 1/8 - 15.2

Fin pitch - 15.2 per inch
Plate spacing - b=0.414 in.
Fin length - 0.125 in.
Fins staggered symmetrically
Flow passage hydraulic diameter - $4r_h$=0.00868 ft.
Fin metal thickness - 0.006 in.
Total heat transfer area/volume between plates - β=417 ft.^{2}/ft.^{3}
Fin area/total area - 0.873

Note: Fin leading and trailing edges slightly scarfed from fin cutting operation. Friction factors may be lower with clean fins.

W. M. Kays and A. L. London, Compact Heat Exchangers, The National Press, Palo Alto, Calif., 1955 (reproduced by permission).

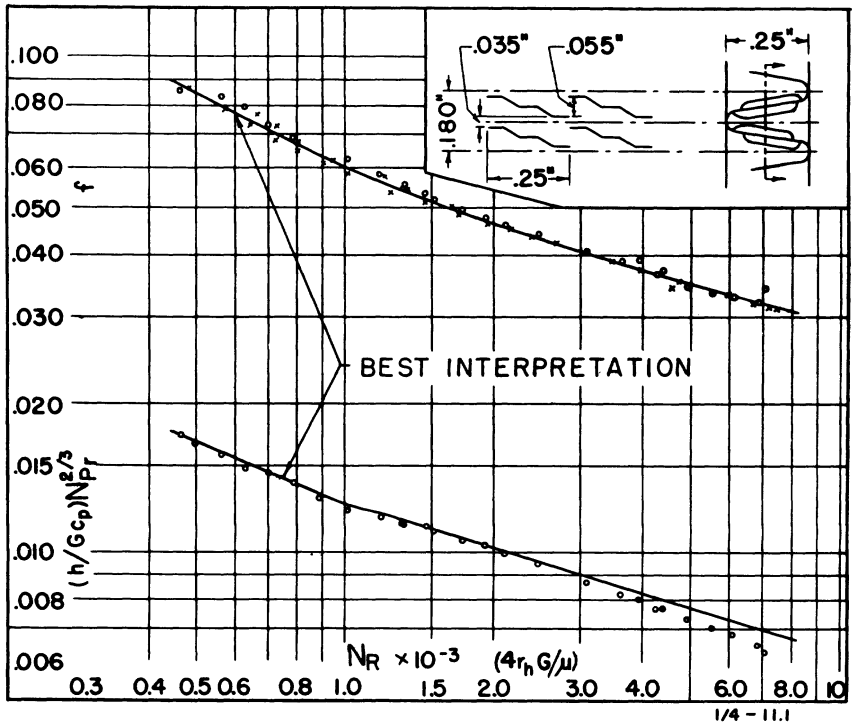

Fig. 15.

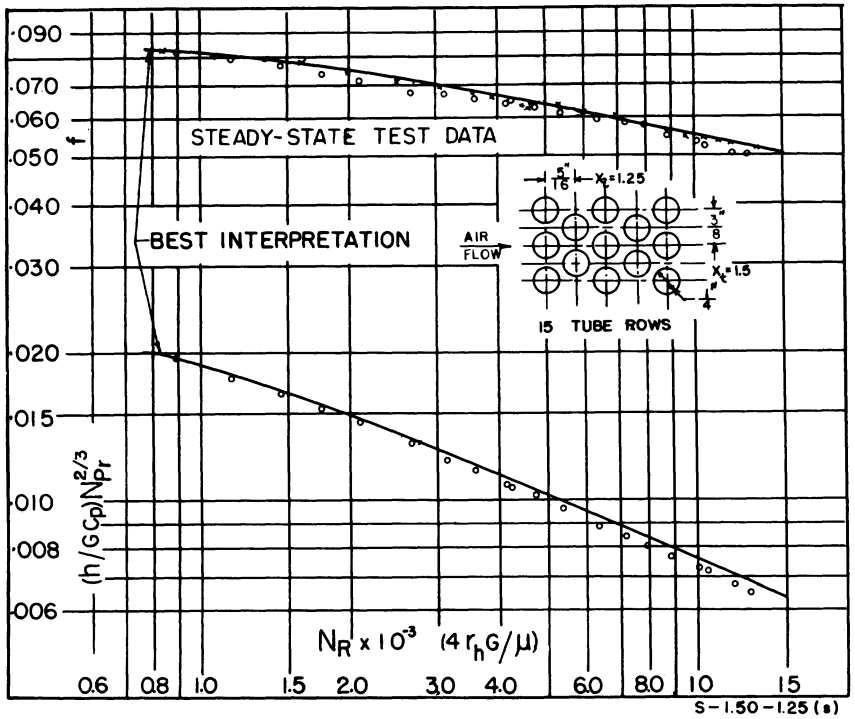

Fig. 16.

LOUVERED PLATE-FIN
SURFACE 1/4 - 11.1

Fin pitch - 11.1 per inch
Plate spacing - b=0.250 in.
Louver spacing - 0.250 in
Fin gap - 0.035 in.
Louver gap - 0.055 in.
Flow passage hydraulic diameter - $4r_h$=0.01012 ft.
Fin metal thickness - 0.006 in.
Total heat transfer area/volume between plates - β=367 ft.^{2}/ft.^{3}
Fin area/total area - 0.756

FLOW NORMAL TO A STAGGERED TUBE BANK
(Steady-state tests)
SURFACE S-1.50-1.25(s)

Tube outside diameter - 0.250 in.
Hydraulic diameter - $4r_h$=0.0166 ft.
Free-flow area/frontal area - σ=0.333
Heat transfer area/total volume - α=80.3 ft.^{2}/ft.^{3}

Note: Minimum free-flow area is in spaces transverse to flow.

W. M. Kays and A. L. London, Compact Heat Exchangers, The National Press, Palo Alto, Calif., 1955 (reproduced by permission).

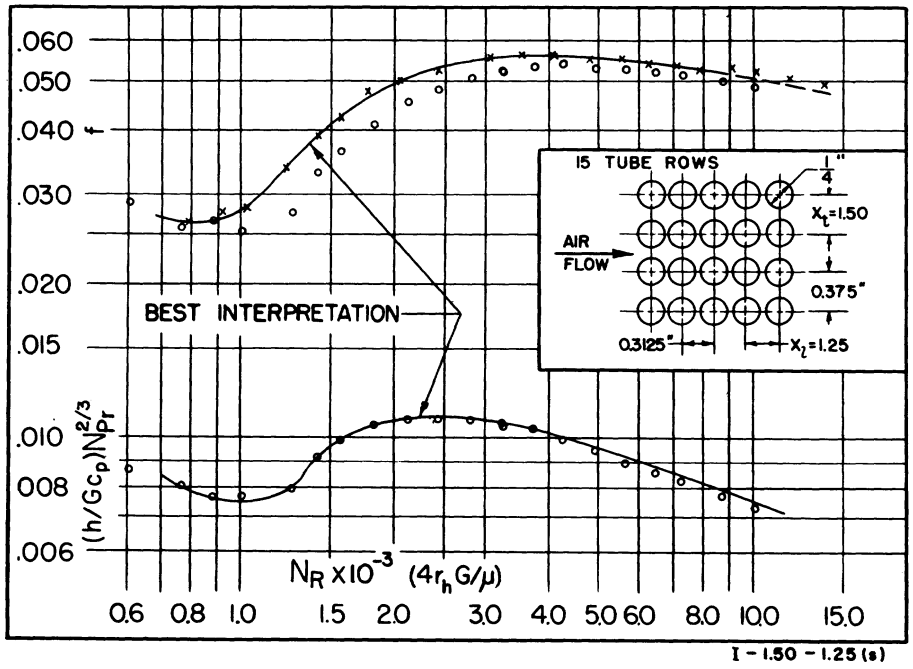

Fig. 17.

FLOW NORMAL TO AN IN-LINE TUBE BANK
(Steady-state tests)
SURFACE I-1.50-1.25(s)

Tube outside diameter - 0.250 in.
Hydraulic diameter - $4r_h$=0.0166 ft.
Free-flow area/frontal area - σ=0.338
Heat transfer area/total volume - α =80.4 $ft.^2/ft.^3$

W. M. Kays and A. L. London, Compact Heat Exchangers, The National Press, Palo Alto, Calif., 1955 (reproduced by permission).

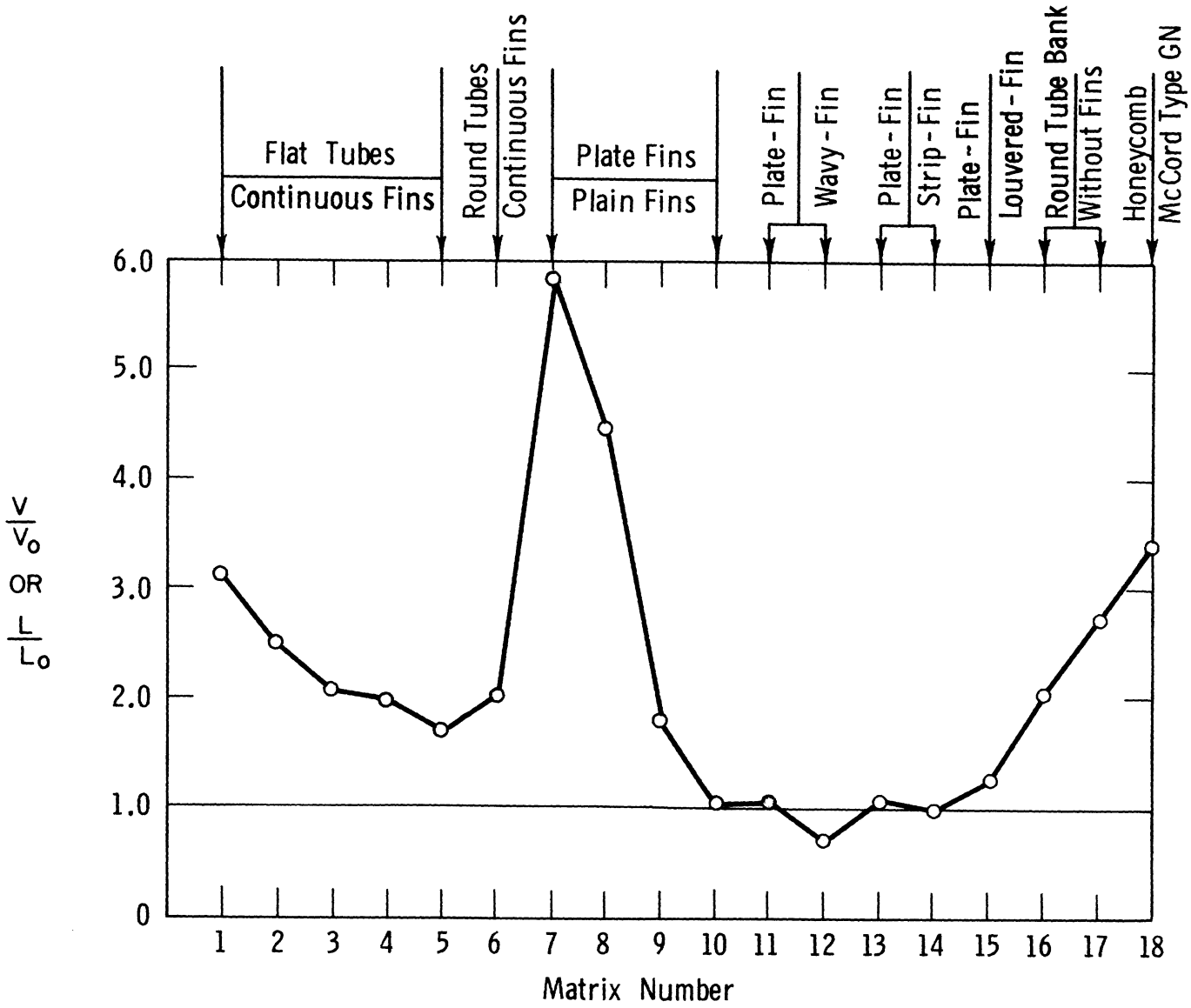
Flat Tubes
Continuous Fins
Round Tubes
Continuous Fins
Plate Fins
Plain Fins
Plate - Fin
Wavy - Fin
Plate - Fin
Strip - Fin
Plate - Fin
Louvered - Fin
Round Tube Bank
Without Fins
Honeycomb
McCord Type GN
6.0
5.0
4.0
3.0
2.0
1.0
0
V/Vo
OR
L/Lo
1 2 3 4 5 6 7 8 9 10 11 12 13 14 15 16 17 18
Matrix Number

Fig. 18.

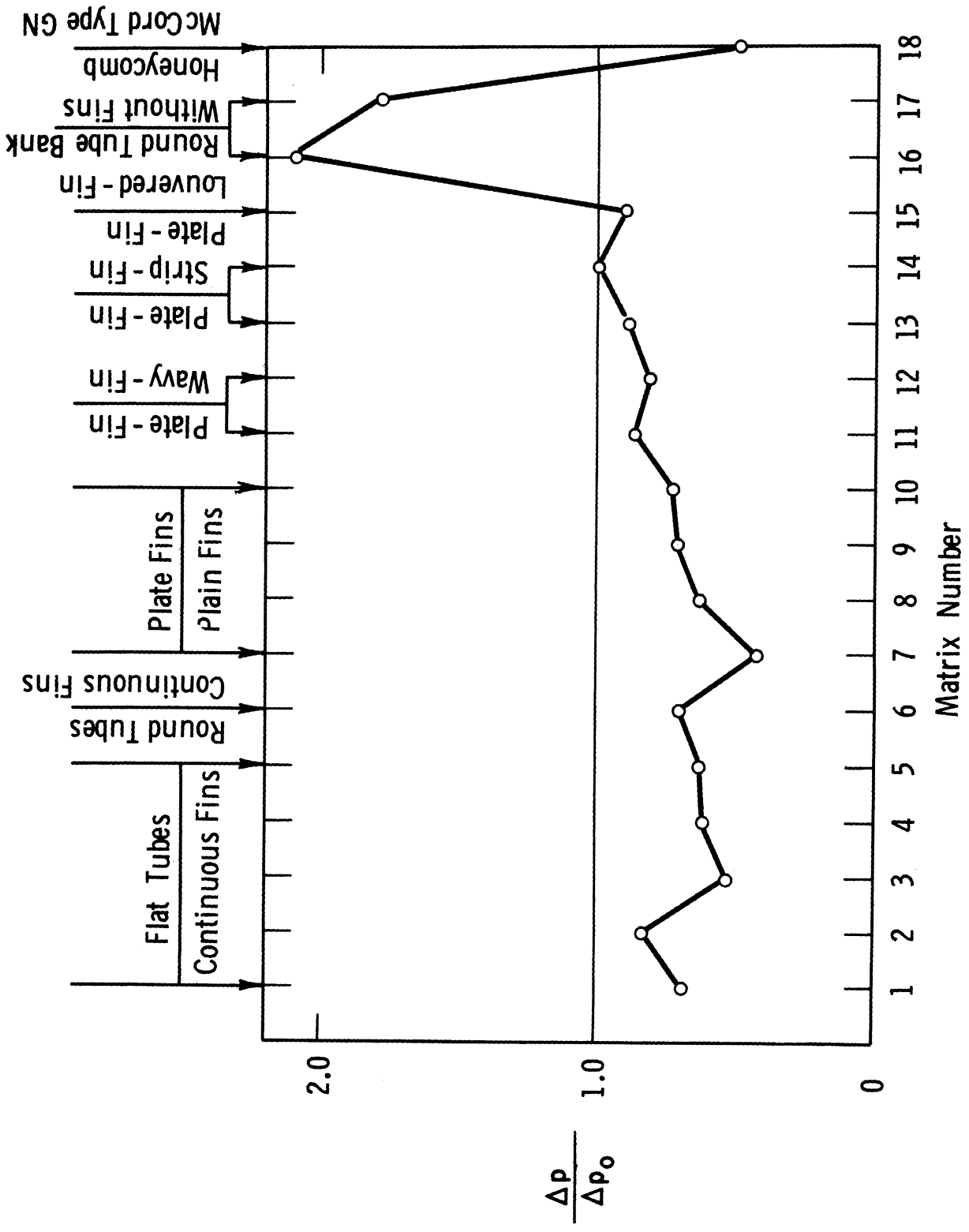
McCord Type GN
Honeycomb
Without Fins
Round Tube Bank
Louvered - Fin
Plate - Fin
Strip - Fin
Plate - Fin
Wavy - Fin
Plate - Fin
Plate Fins
Plain Fins
Continuous Fins
Round Tubes
Flat Tubes
Continuous Fins
2.0
1.0
0
$\frac{\Delta p}{\Delta p_o}$
1 2 3 4 5 6 7 8 9 10 11 12 13 14 15 16 17 18
Matrix Number

Fig. 19.

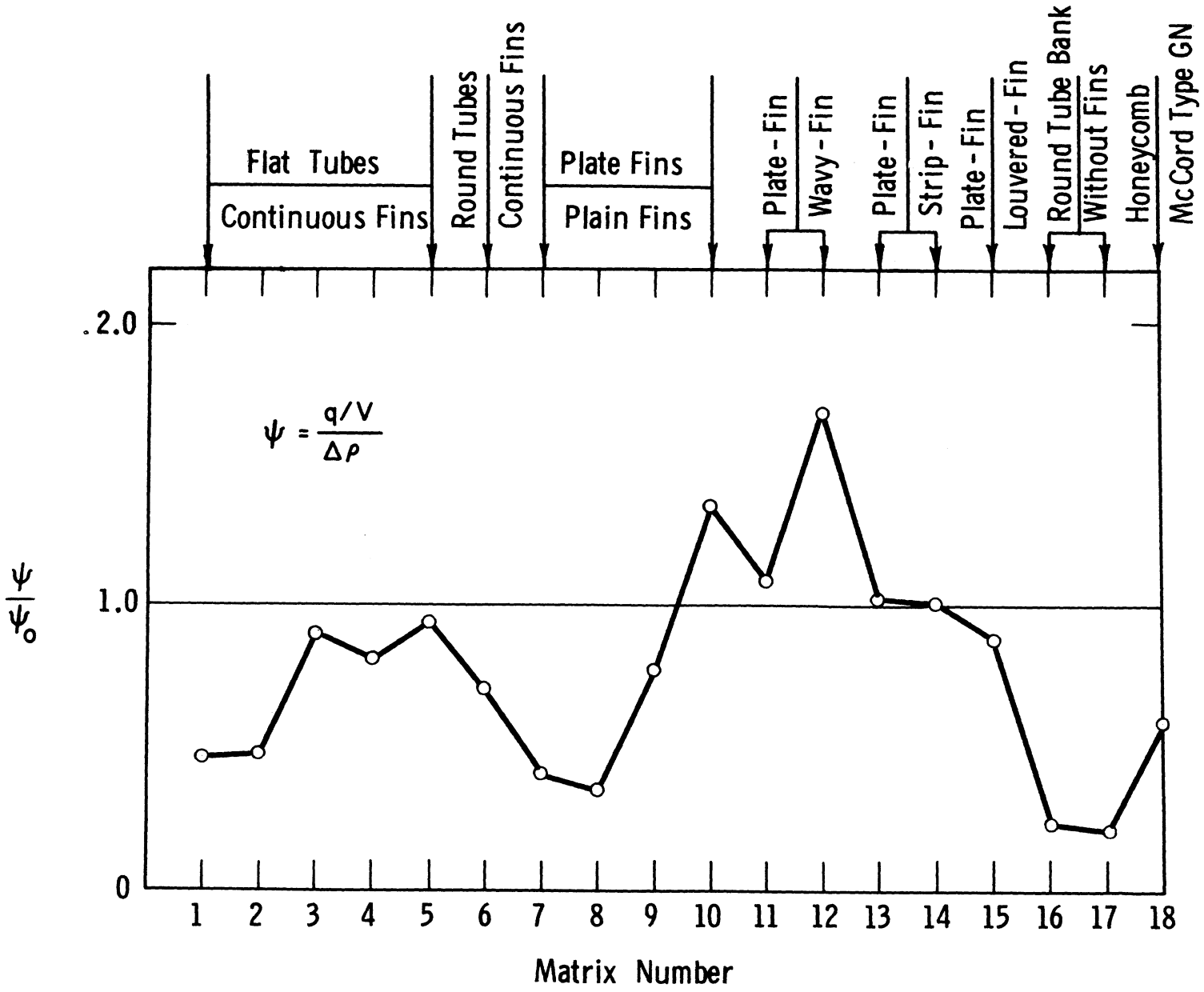
Flat Tubes
Continuous Fins
Round Tubes
Continuous Fins
Plate Fins
Plain Fins
Plate - Fin
Wavy - Fin
Plate - Fin
Strip - Fin
Plate - Fin
Louvered - Fin
Round Tube Bank
Without Fins
Honeycomb
McCord Type GN
2.0
1.0
0
$\psi = \frac{q/V}{\Delta p}$
$\frac{\psi}{\psi_o}$
1 2 3 4 5 6 7 8 9 10 11 12 13 14 15 16 17 18
Matrix Number

Fig. 20.

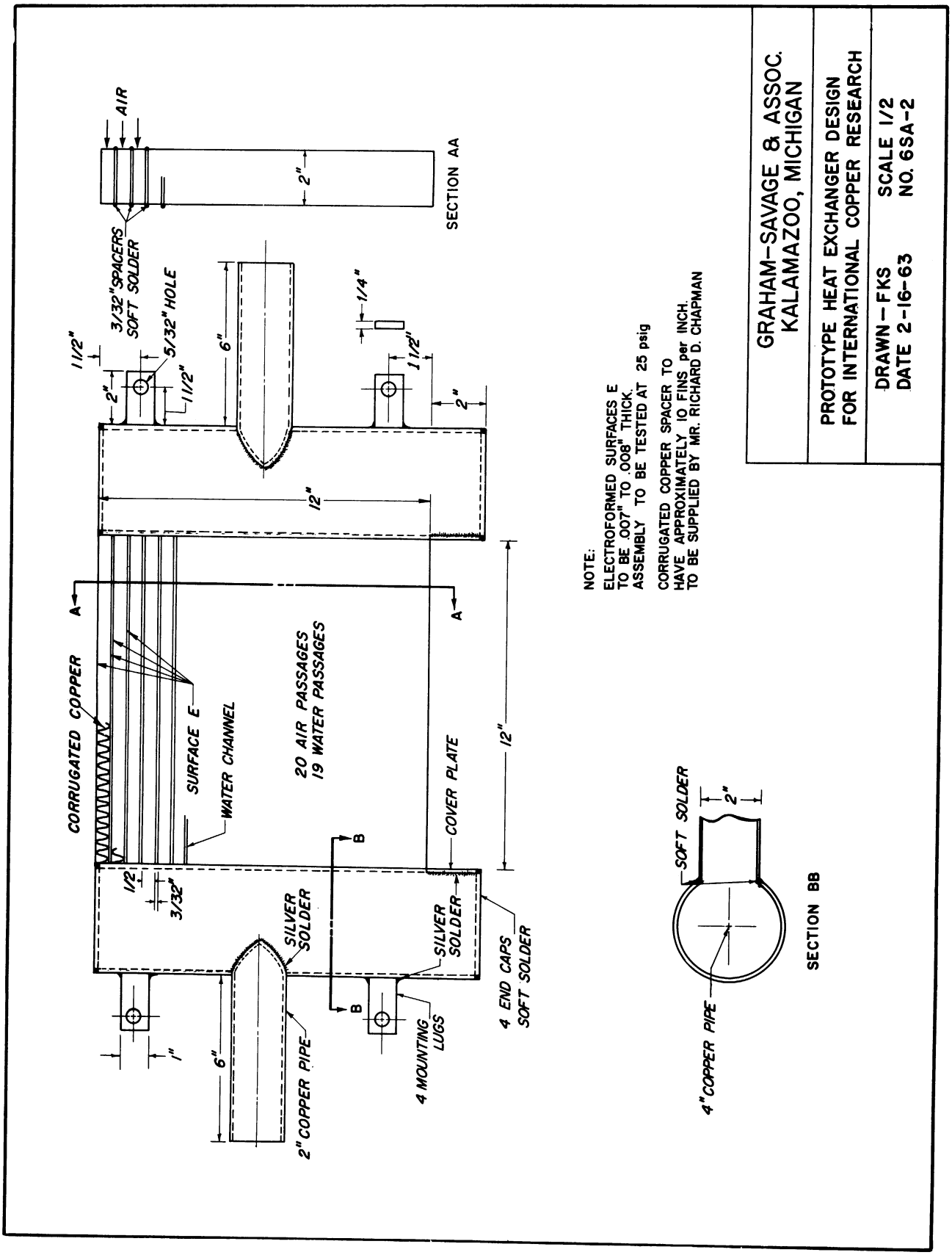
AIR
2"
SECTION AA
3/32" SPACERS SOFT SOLDER
5/32" HOLE
1 1/2"
2"
6"
1/4"
1 1/2"
2"
12"
A
A
CORRUGATED COPPER
SURFACE E
WATER CHANNEL
20 AIR PASSAGES
19 WATER PASSAGES
COVER PLATE
12"
1/2
3/32"
B
B
SILVER SOLDER
SILVER SOLDER
4 END CAPS SOFT SOLDER
1"
6"
2" COPPER PIPE
4 MOUNTING LUGS
NOTE:
ELECTROFORMED SURFACES E TO BE .007" TO .008" THICK. ASSEMBLY TO BE TESTED AT 25 psig
CORRUGATED COPPER SPACER TO HAVE APPROXIMATELY 10 FINS per INCH. TO BE SUPPLIED BY MR. RICHARD D. CHAPMAN
SOFT SOLDER
2"
4" COPPER PIPE
SECTION BB
GRAHAM-SAVAGE & ASSOC.
KALAMAZOO, MICHIGAN
PROTOTYPE HEAT EXCHANGER DESIGN
FOR INTERNATIONAL COPPER RESEARCH
DRAWN - FKS
DATE 2-16-63
SCALE 1/2
NO. 6SA-2

Fig. 21.

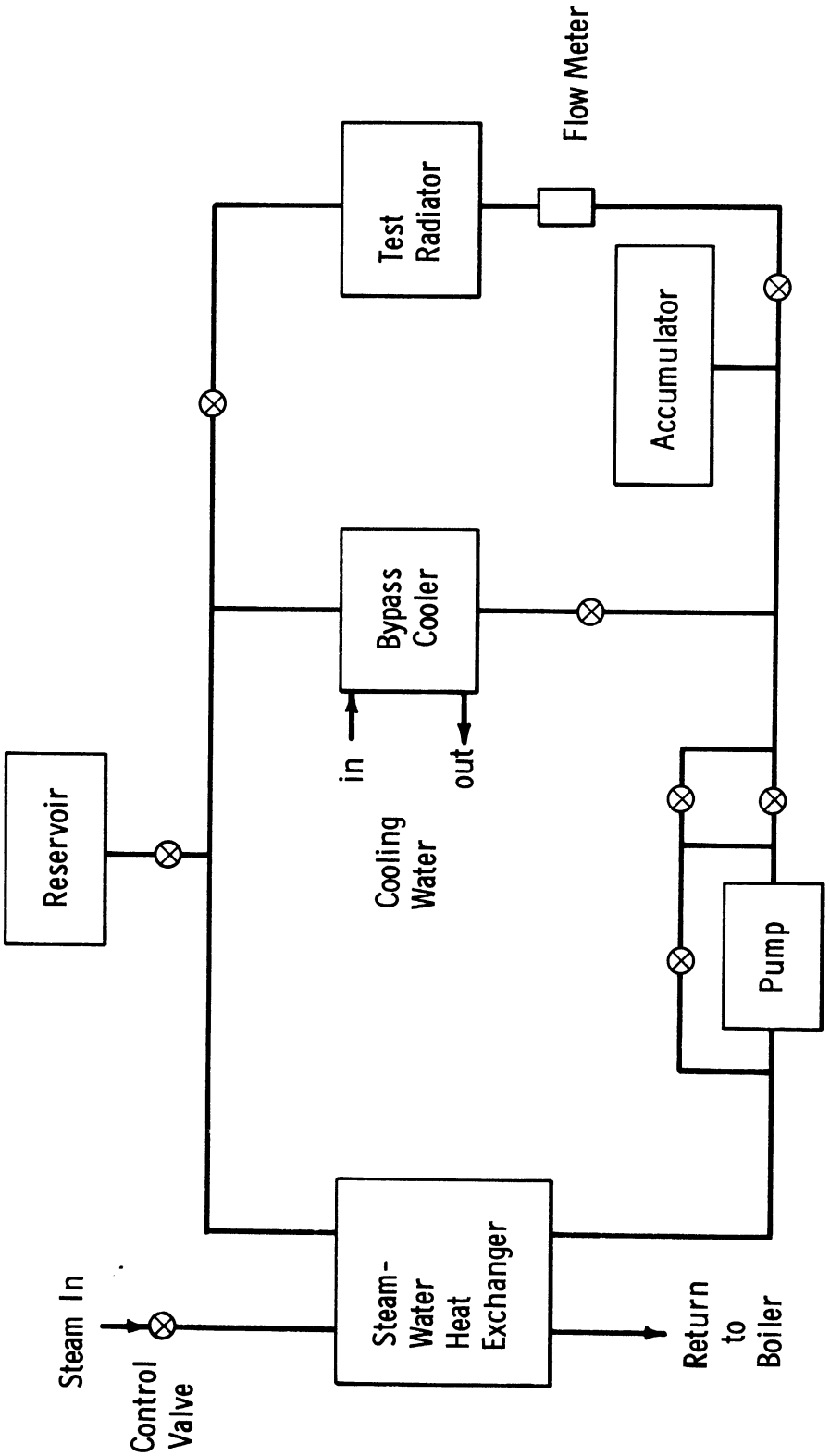
Steam In
Control Valve
Steam-Water Heat Exchanger
Return to Boiler
Reservoir
Cooling Water
in
out
Bypass Cooler
Test Radiator
Flow Meter
Accumulator
Pump

Fig. 22.

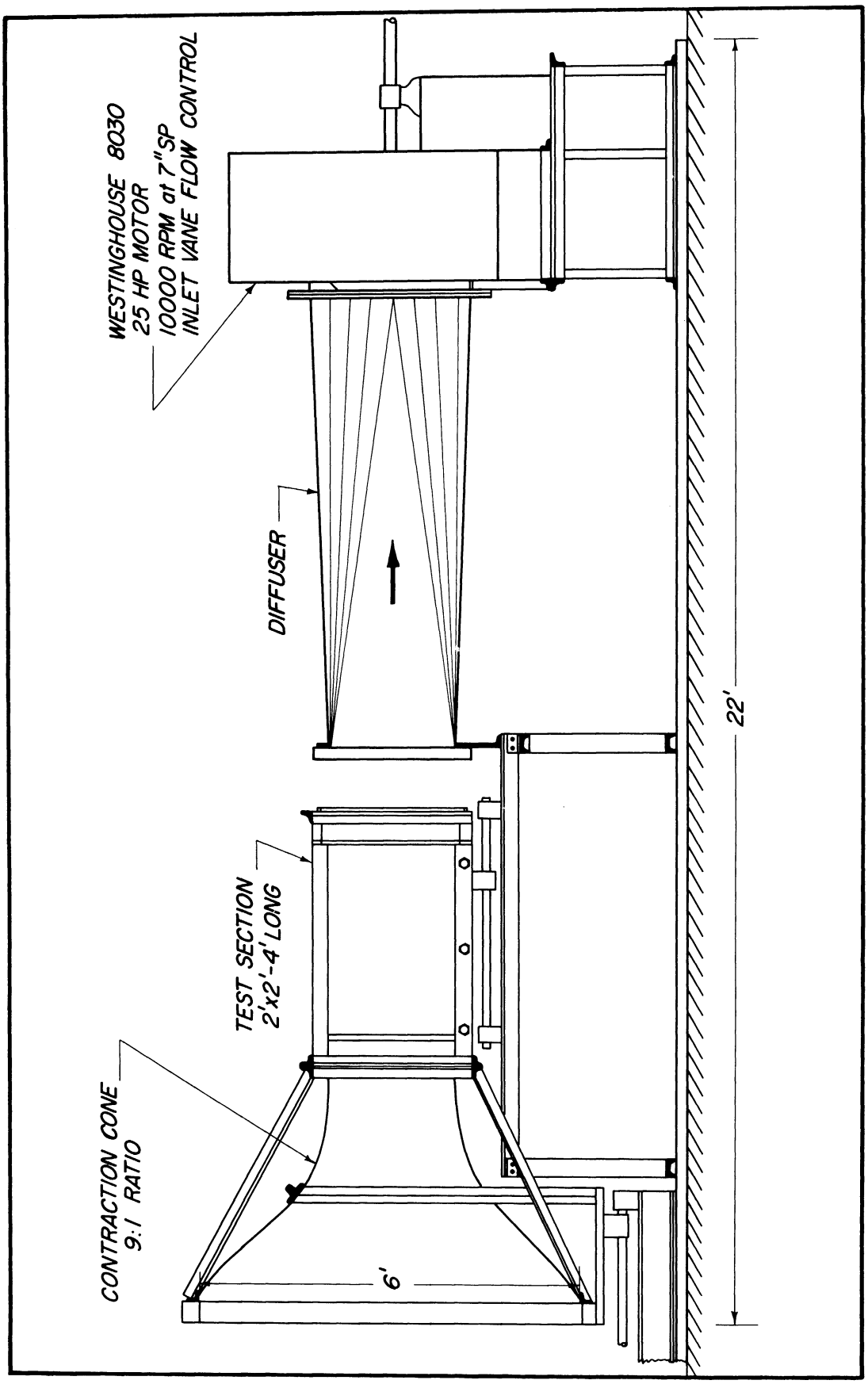
WESTINGHOUSE 8030
25 HP MOTOR
10000 RPM at 7" SP
INLET VANE FLOW CONTROL
DIFFUSER
TEST SECTION
2'x2'-4' LONG
CONTRACTION CONE
9:1 RATIO
6'
22'

Fig. 23.

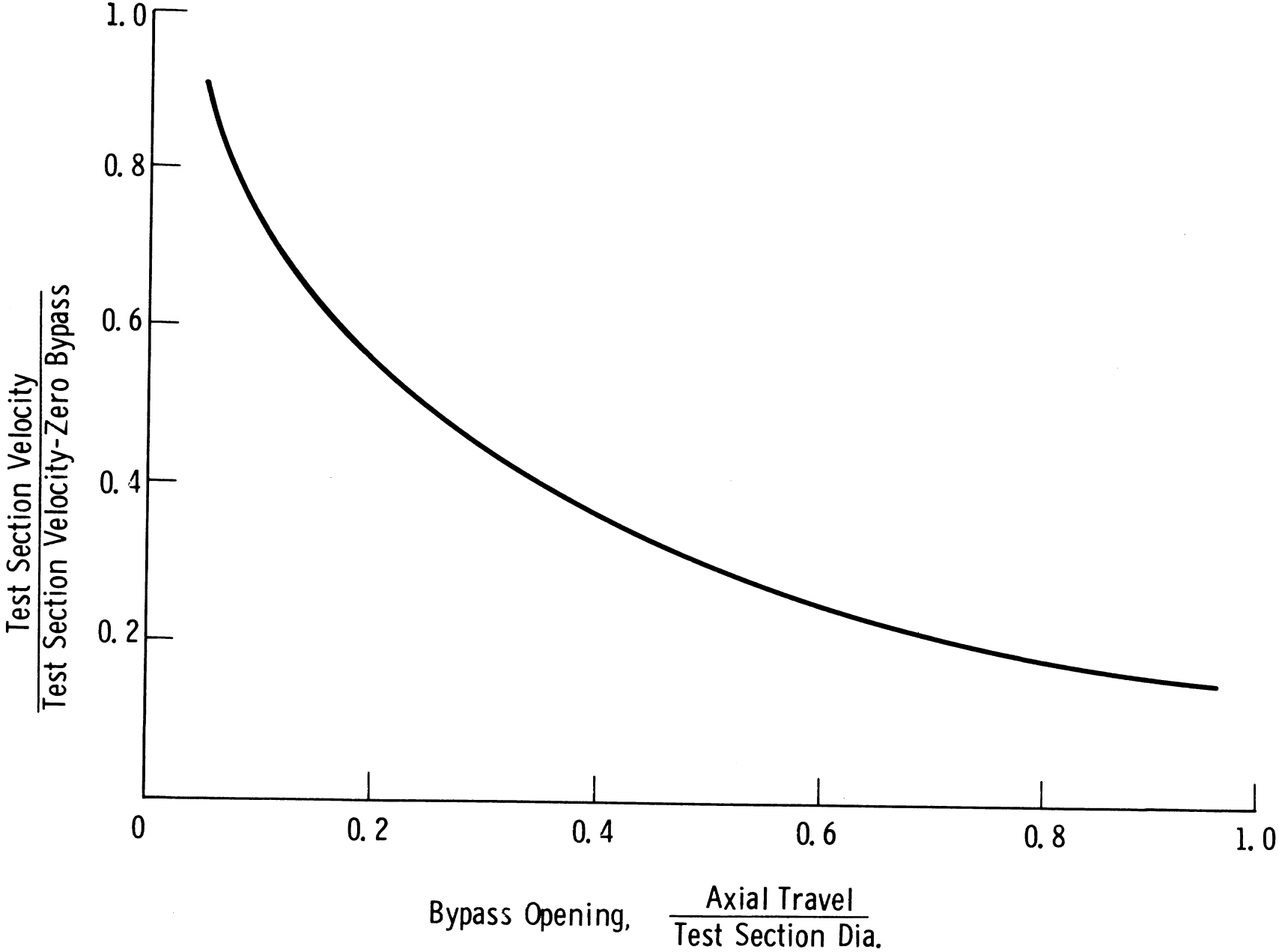
1.0
0.8
0.6
0.4
0.2
0
0.2
0.4
0.6
0.8
1.0
Test Section Velocity / Test Section Velocity-Zero Bypass
Bypass Opening, Axial Travel / Test Section Dia.

Fig. 24.

Match Point	Fan Speed	Bypass	Inlet Vanes
A	100	0	Full Open
B	100	0	Part Closed
C	100	Part Open	Full Open
D	100	Part Open	Part Closed
E	50	0	Full Open
F	50	Part Open	Full Open

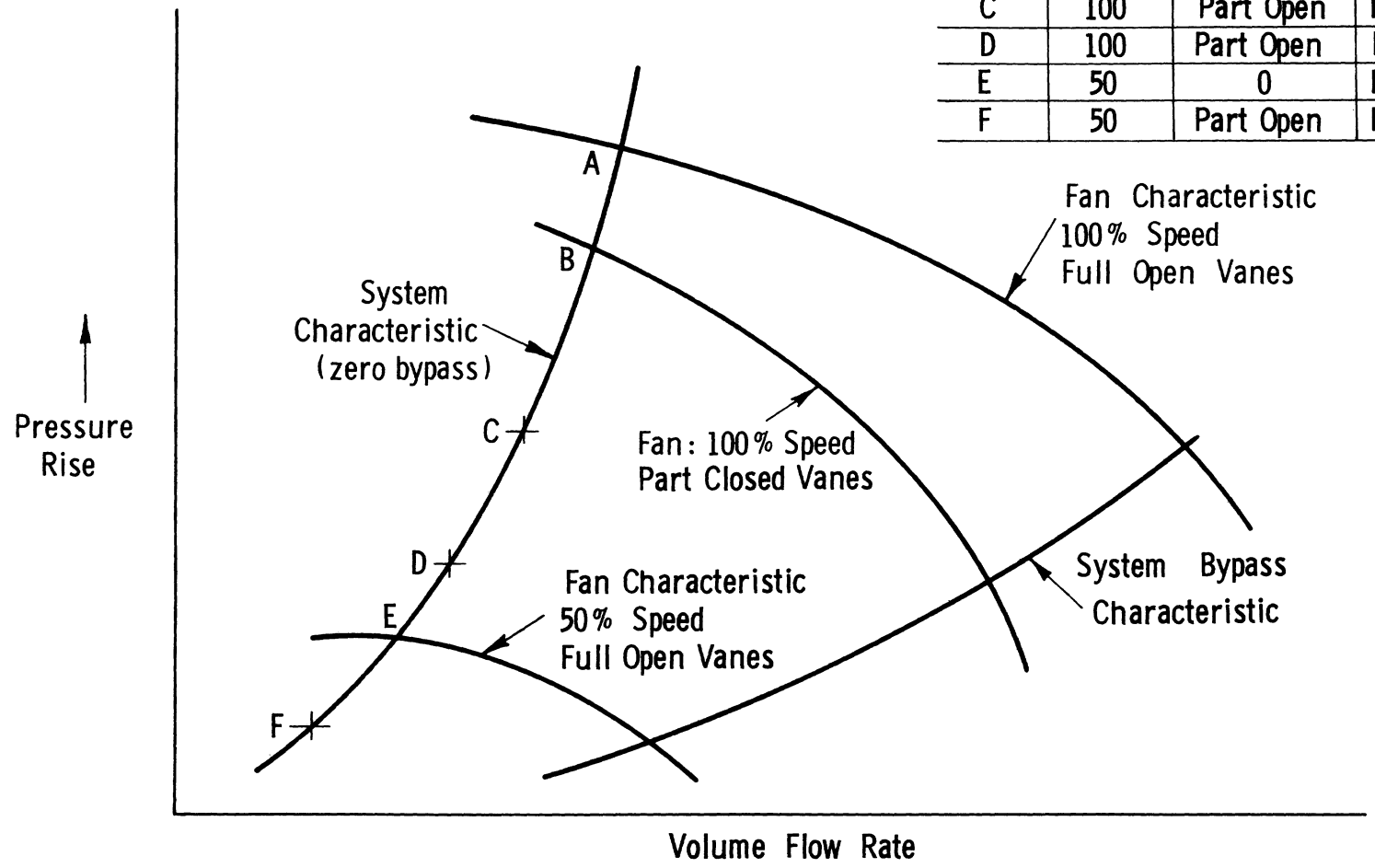

Fig. 25.

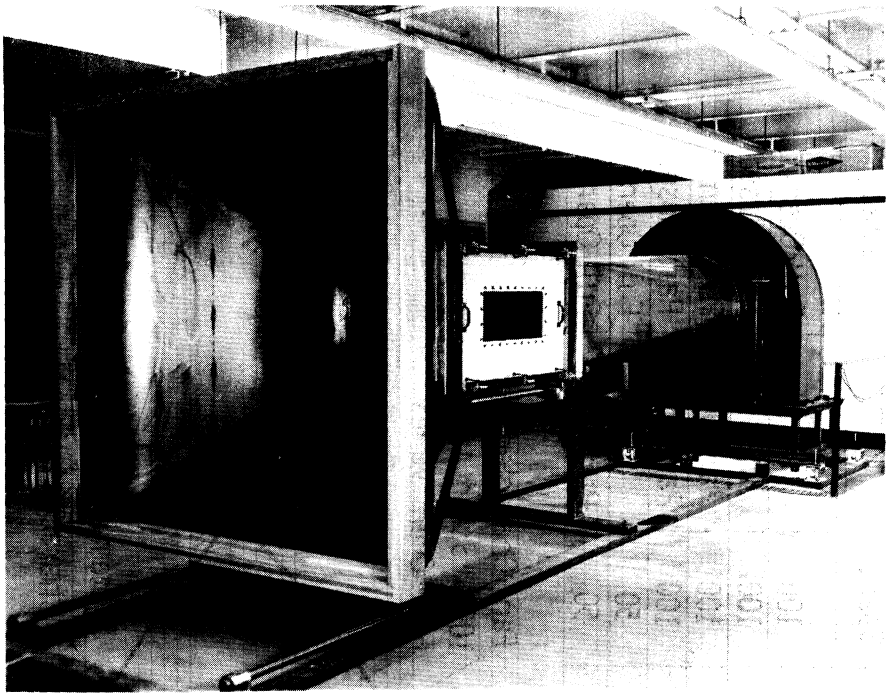

Fig. 26. Wind tunnel.

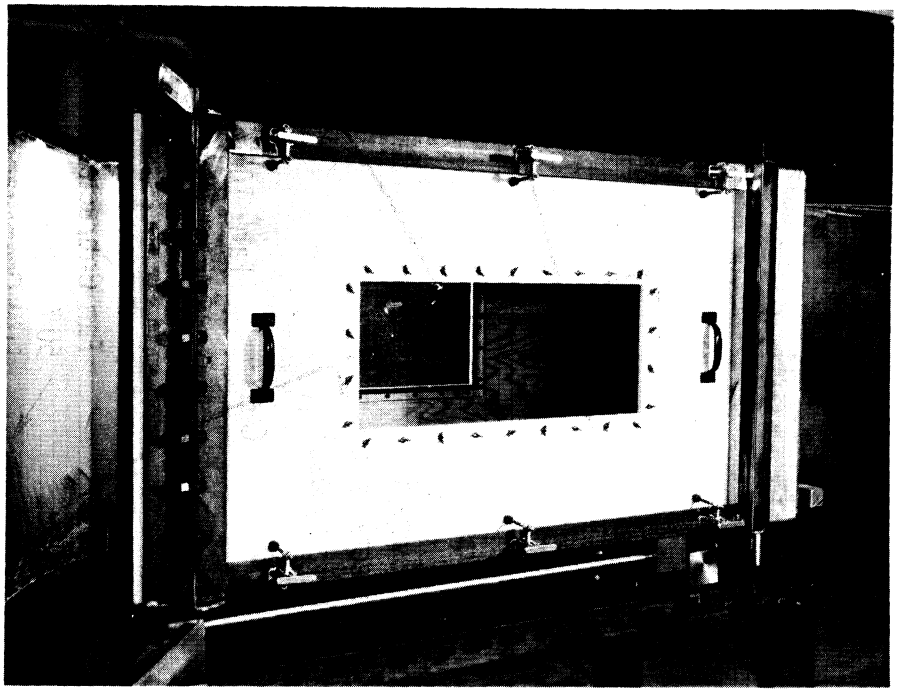

Fig. 27. Wind tunnel test section showing access panel.

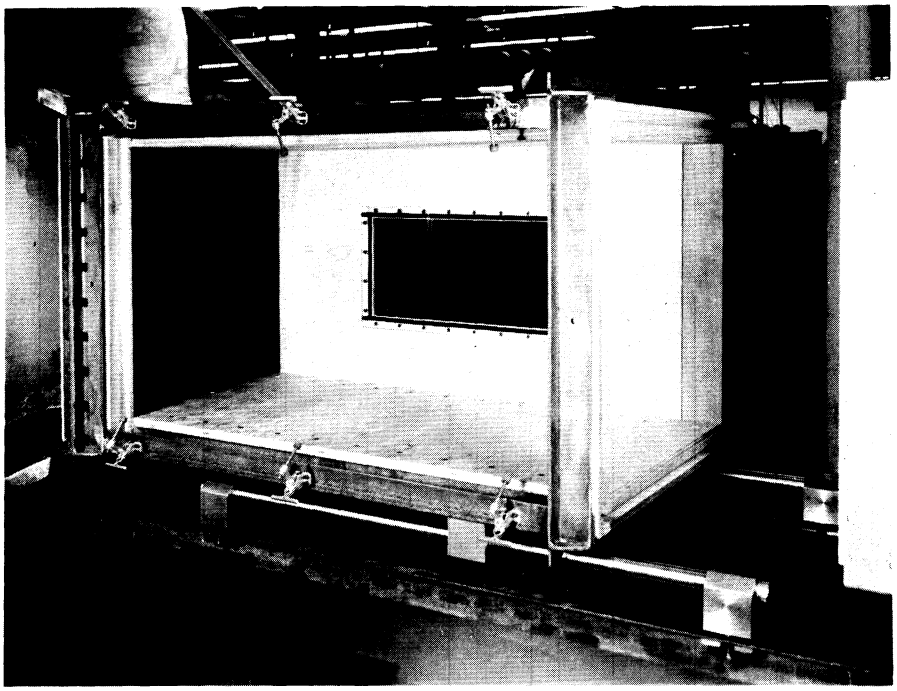

Fig. 28. Wind tunnel test section with access panel removed and air bleed shown.

Fig. 29. Microstructure of "0.010 in." copper, NH_4OH, H_2O_2 etch, magnification 100x.

Fig. 30. Microstructure of "0.010 in." copper, NH_4OH, H_2O_2 etch, magnification 500x.

Fig. 31. Microstructure of "0.020 in." copper, NH_4OH, H_2O_2 etch, magnification 100x.

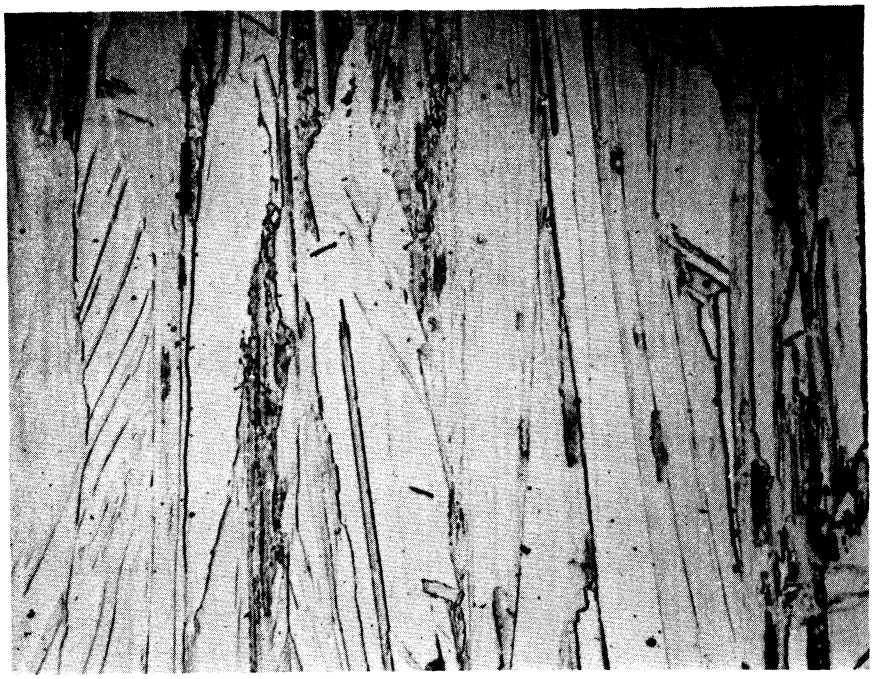

Fig. 32. Microstructure of "0.020 in." copper, NH_4OH, H_2O_2 etch, magnification 500x.

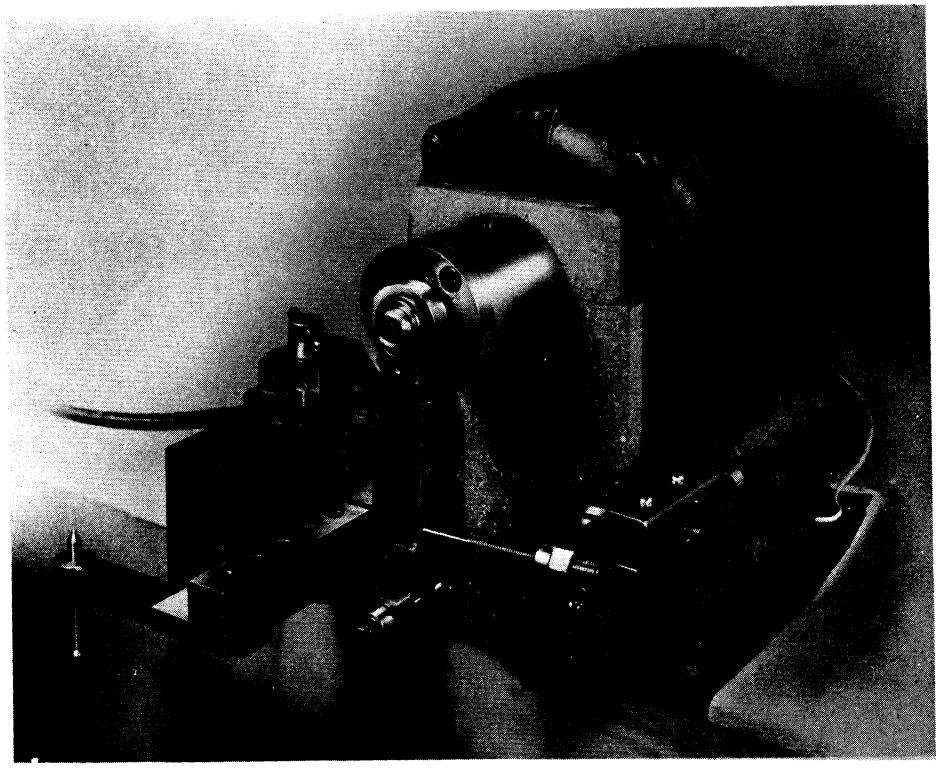

Fig. 33. Krouse fatigue testing machines.